Multiphase Flow Equations for Modeling Tar Production from Biomass Particle Pyrolysis in a Fluidized Bed Reactor

D. Lathouwers and J. Bellan
Jet Propulsion Laboratory
California Institute of Technology
Pasadena, CA 91109

Abstract

A general model is presented for mathematically describing the physics and chemistry of biomass pyrolysis in a fluidized bed reactor. A three fluid model (gas, sand, biomass) is derived by taking suitable ensemble averages of the local gas and particle dynamical equations. The turbulent motion of the gas phase is predicted by a turbulence model augmented with additional terms accounting for the dispersed phase interaction. Closure of the solid phase transport equations is provided in terms of the separate distribution functions for the sand and biomass respectively. Interparticle collisions are described in the framework of the kinetic theory of dense gases using inelastic rigid sphere models. Additional relations are provided for the interphase mass, momentum and energy exchange terms. The most important novelties of this model compared to existing ones are: (i) the modeling of the usually neglected stress tensor resulting from sand-biomass collisions, (ii) the modeling of heat transfer between phases, as well as that resulting from direct particle contacting, and (iii) the modeling of particulate phase, multiple chemical reactions and the resulting mass transfer between phases. Finally, a novel numerical algorithm is described to solve the resulting set of equations and some initial results are discussed.

1 Introduction

1.1 Biomass pyrolysis and model requirements

Biomass pyrolysis involves the heating of raw biomass or organic waste in the absence of an oxidizer in order to extract reaction products for subsequent processing. The interest in clean hydrogen fuel production has triggered the interest in high temperature biomass pyrolysis and is aimed at maximizing tar and gas yields while simultaneously minimizing char formation. Among several rector geometries, the vortex reactor and the bubbling fluidized bed are considered at NREL as alternatives for commercial pyrolysis. The vortex reactor was studied earlier by coupling a detailed model for pyrolysis to a fluid dynamics model of the vortex reactor (Miller and Bellan, 1998). A similarly detailed study of the pyrolysis conditions in a bubbling (or circulating) fluidized bed is not available in literature.

Any comprehensive model for biomass pyrolysis in a process reactor consists of basically two main components: (i) a kinetics scheme for pyrolysis, and (ii) a fluid dynamical description of the chemical reactor. These two model components both need to be of sufficient accuracy for accurate

predictions of product yield, and to allow for sensitivity studies for the determination of optimal operating conditions. It is only recently that a complete kinetics model was devised for general biomass feedstocks (Miller and Bellan, 1997). As far as the fluid dynamics of fluidized bed reactors is concerned, it is poorly understood although some progress has been made in recent years in the area of qualitative predictions.

To appreciate some of the difficulties presented in this area we now discuss the physical mechanisms involved in biomass pyrolysis in a fluidized system. Basically the system consists of a (cylindrical) geometry partially filled with sand. The sand's main purpose is to provide a large heat reservoir to keep the mean temperature of the bed reasonably constant. In turn, heat has to be provided to the sand as pyrolysis is an endothermic reaction extracting heat from the sand. This is done in two ways: heating the walls of the reactor and the injection of steam (or another nonreacting gas) which is also used to fluidize the sand. Both the speed at which pyrolysis can occur as well as the reactive products that are formed depend strongly on temperature. At high temperature, pyrolysis is fast and mainly tar and gas are formed, whereas at low temperatures, pyrolysis is very slow and leads mainly to char formation; as already stated, our interest is in the high temperature regime. The particle temperature is therefore a crucial factor in obtaining the right product formation. Physically, heat transfer to the biomass particles is accomplished in two ways: (i) interaction with the surrounding gas flow, and (ii) heat transfer through direct contact with another particle (sand or another biomass particle). It is obvious that the relative velocity with the surrounding flow and contact area are important parameters with respect to these mechanisms.

The injection of steam fluidizes the sand and the biomass particles leading to a violent gas and solids flow pattern in the reactor, with both locally dense and void regions. An overall circulative complex flow occurs explaining this mixing behavior. The gas flow in the reactor is turbulent and interacts with the particles in a pseudo-random manner. The gas phase turbulence is in part responsible for affecting the particle velocity fluctuations which in turn affect the collisions between particles. The extent to which this interaction happens depends on the solid particle properties and the turbulence. The main mechanism responsible for collisions is shear which is discussed below. The final role of the gas phase is in the removal of gaseous products such as the condensable tar.

The sand and biomass particles are of unequal size and density (and even shape). In general, this causes segregation of the sand and biomass particles which in turn may lead to inhomogeneous temperature distributions in the biomass. As the reaction rates are nonlinear in temperature, this distribution has an effect on tar collection efficiency. Further, note that the segregation depends on time as the biomass particle's mass changes as pyrolysis proceeds.

It is clear from the above discussion that at least the following building blocks need to be included in a simulation model for biomass pyrolysis: (i) separate hydrodynamic equations (mass, momentum and energy) for solids and gas, (ii) solid species and gas species equations along with the kinetics model discussed earlier, (iii) heat transfer between both solids and the gas phase, (iv) heat transfer through direct particle contact (collisional and/or sliding contacts), (v) gas phase turbulence model.

At present there is no complete model available considering all of the above effects simultaneously.

1.2 Modeling status of granular flows

In the present subsection we give a brief outline of models for the prediction of granular multiphase flows. Basically two main simulation methods are available for particle flows, i.e. the Lagrangian and the multifluid scheme. In the Lagrangian scheme, individual particles (or clusters) are tracked through the surrounding gas using an equation of motion. The Eulerian, or multifluid scheme, con-

siders continuum equations for each phase obtained by averaging the local instantaneous equations. Both methods are widely used in the prediction of disperse flows. The present paper concentrates on the Eulerian method as it is much more efficient for industrial size situations where the number of particles and the corresponding details associated with the particle characteristics exceed the computational capacity of modern computers when using Lagrangian schemes.

Two-fluid computations of fluidized systems started in the late 70's. In initial models it was already recognized that a solids 'pressure' was needed in the solids momentum equation to prevent the volume fraction of the solids from reaching impossibly high values (overcompacting). The form of this solids pressure gradient, ∇P_s, in the solids momentum equation was initially highly empirical and was taken to be a strongly increasing function of the solids volume fraction. A severe problem with such models is that the solids viscosity must be specified empirically. In spite of these drawbacks, simulations did show many of the characteristics of fluidized bed systems. Reviews of this type of modelling can be found in Gidaspow (1986). Calculations based on these schemes have prevailed into the early 90's.

At the same time, it was recognized that particles in rapidly sheared dry granular flows, i.e. particle flows without an interstitial gas, had a great similarity with molecules in a dense gas (see Campbell, 1991 for an extensive review). The obvious analogy is that the velocity of each particle can be decomposed in a mean value and a fluctuation leading to the concept of 'granular temperature'. Apart from the obvious analogy, a crucial difference between the two systems is that collisions between the particles in a sheared granular material involve a loss of energy. Consequently, energy must continuously be supplied to the system in order to sustain the particle fluctuating motion.

Ding and Gidaspow (1990) were the first to apply the results from dry granular flow theory to a fluidized bed. The basis of their solids model were the results obtained by Jenkins and Savage (1983) using Maxwellian velocity distributions. Effects of the surrounding gas on particle motion were added as a drag term in the momentum equation and an additional dissipative term in the granular temperature equation. The major advantage of this kinetic model over previous models was that particle-phase viscosities and pressure were predicted by the theory, eliminating the need for more empirical information.

Since Jenkins and Savage, there have been many papers improving on their results; landmark papers include Lun et al. (1984) where the first non-Maxwellian theory is given, and Jenkins and Richman (1985) who extended Grad's Hermite polynomial expansion theory (1949) to dense inelastic interactions. All of these references pertain to dry granular flows. An important extension of Jenkins and Richman's paper was made by Simonin et al. (see e.g. Balzer and Simonin, 1993) who includes the effects of drag and gas phase turbulence in the analysis (also see Peirano 1998).

The biomass pyrolysis requires the description of a binary particulate mixture (sand and biomass). Analysis of binary dry granular mixtures are available in literature but all of these models assume equal granular temperatures and derive mixture mass, momentum and energy equations as is common in kinetic theory (see e.g. Jenkins and Mancini, 1987, 1989). The present study, however, requires separate transport equations for these quantities. Note that the equal granular temperature assumption is justified when the collision frequency is high enough to equilibrate the granular temperatures or when the mass ratio is not too high. The more general analysis of unequal temperatures includes the equal temperature case as limit behavior. Finally, note that the present authors know of only a single reference where an the actual binary mixture computation is performed (Mathiesen, 1996).

1.3 Objectives and outline

The previous two sections have listed the requirements that a model should meet and an overview of what is available in literature with regard to hydrodynamics predictions of fluidized beds. As stated, none of the present models meets all the necessary criteria. The main objective of this paper is therefore to present a model of the thermo-fluid dynamics of a fluidized bed reactor that is sufficiently robust to include the aforementioned physical mechanisms. In particular, the sand and biomass 'phases' are governed by separate hydrodynamic equations derived from an appropriate kinetic theory. Heat transfer between all phases is modeled, and occurs either through the gas or through direct particle contact. Further, the model is combined with a detailed biomass kinetics model making possible the prediction of tar and gas collection in the kinetic regime.

The paper is organized as follows: Section 2 presents the complete mathematical model, including a detailed derivation of all the building blocks and modelling steps needed to complete the formulation. The differential equations constituting the model are solved with a new numerical algorithm which is outlined in detail in section 3. Results from a simulation of a simplified fluidized bed are presented in section 4. This simulation is mainly used as validation for the numerical algorithm presented earlier. Section 5 is devoted to conclusions and a discussion of future model extensions.

2 Mathematical model

2.1 Biomass pyrolysis model and phase topology

The particle pyrolysis model employed here is that of the detailed kinetics derived by Miller and Bellan (1997). The kinetics scheme is based on superimposed cellulose, hemicellulose and lignin reactions. This enables the simulation of different biomass feedstock through knowledge of the initial mass composition with respect to these three primary components. Each of the virgin components undergoes the same generic competitive reaction scheme:

$$\begin{aligned}
&\text{virgin}(s) \xrightarrow{K_1} \text{active}(s) \\
&\text{active}(s) \xrightarrow{K_2} \text{tar}(g) \\
&\text{active}(s) \xrightarrow{K_3} X\text{char}(s) + (1-X)\text{gas}(g) \\
&\text{tar}(g) \xrightarrow{K_4} \text{gas}(g)
\end{aligned}$$

As indicated in the above kinetics scheme, the virgin components, the active intermediates and the char are solid phase species, while tar and gas are vapor products; these species are not pure chemical species but represent groups of compounds. All reactions are modelled with first order Arrhenius kinetics; $K_i = A_i \exp(-E_i/RT)$; where the rate constants, A_i, activation energies, E_i for reactions K_1, K_2, K_3 and the mass ratio X are dependent on the particular component, whereas all heats of reaction and secondary tar decomposition parameters (K_4) are independent of the source component.

This kinetics model combined with a porous particle flow dynamics model yielded validated predictions on tar/char yields ranging from the kinetically controlled region (micro particles) to the diffusion controlled limit (macro particles). In the present paper, the biomass pyrolysis is assumed to be kinetically controlled, which simplifies the description of a biomass particle considerably. This assumption may be justified in the dense particulate regime where contact between particles may

induce fragmentation (see Miller and Bellan, 1998, regarding a fragmentation model) and reduce the size of the particles to the point that the internal temperature equilibrates rapidly. Thus, the particle temperature, its mass and composition (global solid mass fractions) completely describe the state of the particle.

The sand and biomass particles are both solid and hence thermodynamically belong to the same phase. They, however, have different physical properties and different temperatures etc. Therefore these particle classes are handled separately as if they were different phases.

2.2 Ensemble averaging

On a local scale, the flow of a gas-particle mixture can be described by the equations of motion of the fluid coupled to the motion of the discrete particles, governed by Newton's law. This description leads to details that are not of immediate interest. By application of an averaging procedure, these details can be filtered out and the result is a set of equations of motion describing the mixture on a macroscopic scale, i.e. the continuum description. A phase ensemble average is used for the continuous phase (that is, the average is defined over all configurations such that at time t the point $\mathbf{x}$ is in the continuous phase) but not for the particle phase. For the particulates we introduce a particle ensemble average where global particle properties are averaged directly. This is attractive when resolution of the detailed degrees of freedom of the particles (e.g. internal temperature profiles or profiles of the internal chemical composition) is undesirable or unnecessary. We closely follow the exposition of Zhang and Prosperetti (1997).

Consider an ensemble of macroscopically identical suspensions of N_s sand particles and N_b biomass particles in a gaseous carrier phase. Also define the total number of particles, $N = N_s + N_b$. Following Zhang and Prosperetti (1997), we define a configuration to be the specific dynamical state of the system at time t. We also define $\mathcal{Z}$ to be the vector specifying the degrees of freedom that uniquely identifies this state. In particular, $\mathcal{Z}$ includes the locations of the particles' centers of mass $\{\mathbf{y}^i, \mathbf{y}^j\}\, i = 1..N_s; j = 1..N_b$, their linear velocities $\{\mathbf{w}^i, \mathbf{w}^j\}$, etc. Note that for an inviscid flow these are sufficient to characterize the complete state of the system. Here, however, $\mathcal{Z}$ must also include degrees of freedom of the continuous phase to fully characterize the system's dynamical state. $P(N_s, N_b; t)$ is defined as the probability density of encountering configuration $\mathcal{Z}$ in the ensemble at time t. $P(N; t) = P(N_s, N_b; t)$ satisfies the following normalization rule

$$\int P(N;t)d\mathcal{Z} = 1 \tag{1}$$

where $d\mathcal{Z}$ is a volume element in phase space. If f is some field quantity, then its ensemble average $< f >$ reads as

$$< f(\mathbf{x},t) >= \int f(\mathbf{x},t)P(N;t)d\mathcal{Z} \tag{2}$$

From this definition it is clear that ensemble averaging commutes with time and space-derivatives, i.e. Leibniz' and Gauss' rules:

$$\begin{aligned} < \nabla f >&= \nabla < f > \\ < \frac{\partial f}{\partial t} >&= \frac{\partial < f >}{\partial t} \end{aligned} \tag{3}$$

In order to be able to derive *phasic* ensemble averages, it is convenient to introduce the phase indicator function $\chi_k(\mathbf{x}, t)$:

$$\chi_k(\mathbf{x},t) = \begin{cases} 1, \text{if} \mathbf{x} \in k \\ 0, \text{otherwise} \end{cases} \tag{4}$$

This function is used to filter out the realizations for which the position $\mathbf{x}$ at time t is not in phase k. A fundamental property of the indicator function is that it is advected at the velocity of the interface, $\mathbf{u}_{ki}$

$$\frac{\partial \chi_k}{\partial t} + \mathbf{u}_{ki} \cdot \nabla \chi_k = 0 \tag{5}$$

This equation is used extensively in the derivation of the average transport equations given in the next section. The gradient of the indicator function is nonzero at points in the mixture that lie on the interface between phase k and the other phases. The components of $\nabla \chi_k$ constitute the unit normal vector at the interface multiplied by a delta function:

$$\nabla \chi_k(\mathbf{x}, t) = \mathbf{n}_k \delta(\mathbf{x} - \mathbf{x}_i) = \mathbf{n}_k \delta \tag{6}$$

where $\mathbf{n}_k$ is the unit normal vector pointing inward with respect to phase k, and the $\mathbf{x}_i$ constitute all points on the interface. The ensemble average of the phase indicator is the probability that a point is in phase k and is defined as the phase fraction α_k

$$\alpha_k(\mathbf{x}, t) = \int \chi_k P d\mathcal{Z} \tag{7}$$

From these definitions, the consistency condition $\sum_k \alpha_k = 1$ follows immediately. The phase ensemble average of a quantity Ψ_k of phase k can now be defined in terms of the probability density and the phase indicator

$$\overline{\Psi}_k(\mathbf{x}, t) = \frac{< \chi_k \Psi_k >}{\alpha_k} = \frac{1}{\alpha_k} \int \chi_k \Psi_k P d\mathcal{Z} \tag{8}$$

This is the average that will be used for averaging the carrier phase variables.

As we mentioned earlier, ensemble averaging commutes with the derivative operator for the mixture as a whole; thus we may write

$$< \chi_k \nabla f_k >= \nabla < \chi_k f_k > - < f_k \nabla \chi_k > \tag{9}$$

Here the term $< f_k \nabla \chi_k >$ represents an interfacial average that leads to a finite contribution in the macroscopic equations.

As the carrier phase is compressible, it is convenient to define a density-weighted average similar to the Favre average:

$$\widetilde{\Psi}_k(\mathbf{x}, t) = \frac{< \chi_k \rho_k \Psi_k >}{\alpha_k \overline{\rho}_k} = \frac{1}{\alpha_k \overline{\rho}_k} \int \chi_k \rho_k \Psi_k P d\mathcal{Z} \tag{10}$$

Similar averages could be defined for the particle phases (see e.g. Drew (1983) for such an approach) where the solid particle is described as a continuum material with certain elastic properties. Such an approach does not treat particles as single entities and makes it more difficult to include particle physics into the model. It is therefore more convenient to recognize that rigid particles can be completely described in terms of their linear and angular velocities. Zhang and Prosperetti (1997) proceed to derive the single particle velocity distribution, by integration of $P(N_s, N_b; t)$. Let $f_k^{(1)}(\mathbf{x}, \mathbf{w}, Y_\xi, T, m, t)$ denote the single particle distribution function of particle class k such that $\mathbf{x}$ is the probable number of particles of class i having their center of mass in the region $[\mathbf{x}, \mathbf{x} + d\mathbf{x}]$, a velocity in the region $[\mathbf{w}, \mathbf{w} + d\mathbf{w}]$, mass in the region $[m, m + dm]$, mass fractions in $[Y_\xi, Y_\xi + dY_\xi]$, and temperature in $[T, T + dT]$. Then f is related to P in the following manner

$$f_k^{(1)}(\mathbf{x}, \mathbf{w}, Y_\xi, T, m, t) = \int P(N_s, N_b; t) d\mathcal{Z}^{N_1} d\mathcal{Z}^{N_k - 1} \tag{11}$$

where the integration is over all degrees of freedom, except those explicitly defining the state of particle 1, i.e. the position of its center of mass, its center of mass velocity, its composition, its temperature, and its mass. The number density, n_k, of particle phase k follows by integration of the single-particle distribution function f_k:

$$n_k(\mathbf{x},t) = \int f_k d\mathbf{w} dY dT dm = \int f_k d\mathcal{Z}^p \tag{12}$$

With the previously derived single-particle distribution, the particle averages may be introduced as follows

$$\overline{\Psi}_k(\mathbf{x},t) = \frac{1}{n_k}\int \Psi_k f_k d\mathcal{Z}^p \tag{13}$$

where $d\mathcal{Z}^p$ is shorthand for the set of integration variables. The mass of the particles need not be a constant, therefore mass weighted averages are also introduced:

$$\widetilde{\Psi}_k(\mathbf{x},t) = \frac{1}{\alpha_k\overline{\rho}_k}\int m_k \Psi_k f_k d\mathcal{Z}^p \tag{14}$$

where

$$\alpha_k\overline{\rho}_k = n_k\overline{m}_k = \int m_k f_k d\mathcal{Z}^p \tag{15}$$

This definition of the mass-weighted particle average is completely comparable to that used for the carrier phase and leads to more convenient forms of the moment equations derived later.

The macroscopic equations contain certain interfacial coupling terms describing the various transfer processes taking place through the interface. As noted, these terms are of the form $< f_k \nabla\chi_k >$ (where f_k is generally a flux). This average is taken over all realizations at a fixed point in space. On the other hand, the particle phase is described by a particle ensemble average. It would seem tempting to equate an interfacial average to the average over the interface of a representative particle. This is however only correct for homogeneous flows. The cause of this difference lies in the positions at which contributions to the average are obtained (the interfacial average having contributions only at the point of interest where an interface exists; the particle average having their center at this point and accumulating contributions from the interfaces belonging to these particles).

Bulthuis (1997) has derived the result that for particles of general shape, the interfacial average can be written as a series expansion of particle averages:

$$< f_k \nabla\chi_k >= n\overline{\int d\mathbf{S} f_k} - \nabla\cdot n\overline{\int d\mathbf{S}\mathbf{s} f_k} + ... \tag{16}$$

where the overbars denote particle ensemble averages, the integrals are over the particle surface and where $\mathbf{s} = \mathbf{x}_i - \mathbf{x}_0$, and $\mathbf{x}_0$ is the center of the particle. The first term of this expansion gives the intuitive equality discussed earlier where the interfacial average is set equal to the surface average of an ensemble of test particles.

An important result is obtained by taking $f_k = 1$:

$$\nabla\alpha_k = \nabla n\tau + ... \tag{17}$$

where τ is the average volume displaced by the particle. This shows that relation (15) is not exact in the general case of inhomogeneous flow. The macroscopic equations derived from these theorems are therefore valid only in flows exhibiting mild gradients (a condition that is assumed below as it is inherent in all derivations of particle conservation equations based upon hard sphere kinetic theories, see Jenkins and Savage, 1983).

2.3 Averaged equations for the gas phase

2.3.1 Local instantaneous flow description

The starting point for the derivation of the macroscopic carrier phase equations are the local instantaneous equations in the gas phase expressing the conservation of mass, momentum, energy, and species mass fractions:

$$\frac{\partial \rho_g}{\partial t} + \nabla \cdot (\rho \mathbf{u})_g = 0 \tag{18}$$

$$\frac{\partial (\rho \mathbf{u})_g}{\partial t} + \nabla \cdot (\rho \mathbf{u}\mathbf{u})_g = \nabla \cdot \boldsymbol{\sigma}_g + \rho_g \mathbf{g} \tag{19}$$

$$\rho_g \frac{Dh_g}{Dt} = -\nabla \cdot \mathbf{q}_g + \frac{Dp_g}{Dt} + \sum S_i \Delta h_i - (\boldsymbol{\tau} : \nabla \mathbf{u})_g \tag{20}$$

$$\frac{\partial (\rho Y_\xi)_g}{\partial t} + \nabla \cdot (\rho \mathbf{u} Y_\xi)_g = -\nabla \cdot \mathbf{j}_\xi + \rho_g R_{g\xi} \tag{21}$$

Here, we assume the gas phase to behave as a simple Newtonian fluid:

$$\boldsymbol{\sigma}_g = -p_g \mathbf{I} + \mu[(\nabla \mathbf{u}_g) + (\nabla \mathbf{u}_g)^{\mathrm{T}} - 2/3(\nabla \cdot \mathbf{u}_g)] \tag{22}$$

and further assume the gas mixture to be ideal:

$$p_g = \rho_g \sum_\xi \frac{Y_\xi}{W_\xi} R^0 T_g \tag{23}$$

where R^0 denotes the universal gas constant and W_ξ is the molecular weight of specie ξ. The specie flux $\mathbf{j}_\xi$ is written as a simple gradient diffusion (Fickian) relation neglecting all multicomponent behavior:

$$\mathbf{j}_\xi = -\rho_g \mathcal{D}_\xi \nabla Y_\xi \tag{24}$$

The heat flux $\mathbf{q}_g$ is given by

$$\mathbf{q}_g = -\lambda_g \nabla T_g - \sum_\xi h_\xi \mathbf{j}_\xi \tag{25}$$

where the second term represents the interdiffusion of heat. This set of equations (supplemented with appropriate boundary conditions) is a closed system for the local description of the gas phase.

2.3.2 Macroscopic equations

The macroscopic gas phase equations are derived by multiplying the local instantaneous transport equations of the previous section by the gas phase indicator χ_g and ensemble averaging. After some manipulation this yields

$$\frac{\partial (\alpha \overline{\rho})_g}{\partial t} + \nabla \cdot (\alpha \overline{\rho} \widetilde{\mathbf{u}})_g = \Gamma_g \tag{26}$$

$$\frac{\partial (\alpha \overline{\rho} \mathbf{u})_g}{\partial t} + \nabla \cdot (\alpha \overline{\rho} \widetilde{\mathbf{u}} \widetilde{\mathbf{u}})_g = \nabla \cdot [\alpha \overline{\boldsymbol{\sigma}} + \boldsymbol{\Sigma}^{\mathrm{Re}}]_g + \alpha_g \overline{\rho}_g \mathbf{g} + \mathbf{M}_g + \Gamma_g \widehat{\mathbf{u}}_g^{\mathrm{i}} \tag{27}$$

$$\overline{\rho}_g \frac{D\widetilde{h}_g}{Dt} = -\nabla \cdot [\alpha \overline{\mathbf{q}} + \mathbf{q}^{\mathrm{Re}}]_g + \sum \overline{S}_i \Delta h_i + F_g + \Gamma_g (\widehat{h}_g^{\mathrm{i}} - \widetilde{h}_g) \tag{28}$$

$$\frac{\partial(\alpha\bar{\rho}\widetilde{Y}_\xi)_g}{\partial t} + \nabla\cdot(\alpha\bar{\rho}\widetilde{\mathbf{u}}\widetilde{Y}_\xi)_g = -\nabla\cdot[\alpha\bar{\mathbf{j}}_{g\xi} + \mathbf{j}_\xi^{\mathrm{Re}}]_g + \alpha_g\bar{\rho}_g\widetilde{R}_{g\xi} + H_{g\xi} + \Gamma_g\widehat{Y}_{g\xi}^i \tag{29}$$

where the effect of pressure and viscous dissipation in the energy equation has been neglected. To keep the expressions tractable, several new variables have been introduced. These can be divided into three groups.

(i) interfacial coupling terms

$$\mathbf{M}_g = -<\boldsymbol{\sigma}_g\cdot\nabla\chi_g> \tag{30}$$

$$H_{g\xi} =<\mathbf{j}_{g\xi}\cdot\nabla\chi_g> \tag{31}$$

$$F_g =<\mathbf{q}_g\cdot\nabla\chi_g> \tag{32}$$

(ii) additional interfacial transfer related to the transfer of mass between phases

$$\Gamma_g =<\rho_g(\mathbf{u}_g-\mathbf{u}_{gi})\cdot\nabla\chi_g> \tag{33}$$

$$\Gamma_g\widehat{\mathbf{u}}_g^i =<\rho_g\mathbf{u}_g(\mathbf{u}_g-\mathbf{u}_{gi})\cdot\nabla\chi_g> \tag{34}$$

$$\Gamma_g\widehat{Y}_{g\xi}^i =<\rho_g\mathbf{Y}_{g\xi}(\mathbf{u}_g-\mathbf{u}_{gi})\cdot\nabla\chi_g> \tag{35}$$

$$\Gamma_g\widehat{h}_g^i =<\rho_g h_g(\mathbf{u}_g-\mathbf{u}_{gi})\cdot\nabla\chi_g> \tag{36}$$

(iii) fluxes related to 'turbulent' fluctuations

$$\boldsymbol{\Sigma}_g^{\mathrm{Re}} = -\frac{<\chi_g\rho_g\mathbf{u}_g'\mathbf{u}_g'>}{\alpha_g} \tag{37}$$

$$\mathbf{j}_{g\xi}^{\mathrm{Re}} = \frac{<\chi_g\rho_g\mathbf{u}_g'Y_{g\xi}'>}{\alpha_g} \tag{38}$$

$$\mathbf{q}_g^{\mathrm{Re}} = \frac{<\chi_g\rho_g\mathbf{u}_g'h_g'>}{\alpha_g} \tag{39}$$

where the fluctuations result from a decomposition of the instantaneous variable into its mean and a fluctuation, e.g. $\mathbf{u}_g = \widetilde{\mathbf{u}}_g + \mathbf{u}_g'$. Owing to the usage of appropriate density-weighted variables, the general form of these transport equations is comparable to their local instantaneous form. The continuity equation contains a single source term, Γ_g, representing the average mass source for the gas phase. There are basically two mechanisms that give rise to stress/flux terms in the averaged equations. The first one initiates in the (averaged) molecular stress/flux terms, $\overline{\boldsymbol{\sigma}}_g$, $\bar{\mathbf{j}}_{g\xi}$ and $\overline{\mathbf{q}}_g$. Note that since the molecular fluxes are linear in gradients of velocity and species mass fractions, these terms are not closed owing to the fact that the derivatives and phase ensemble averaging operators don't commute. The second contribution to stresses/fluxes arises from the nonlinear convective terms in the transport equations: the terms $\boldsymbol{\Sigma}_g^{\mathrm{Re}}$, $\mathbf{j}_{g\xi}^{\mathrm{Re}}$ and $\mathbf{q}_g^{\mathrm{Re}}$ are fully comparable to their counterparts found in single-phase turbulent flows. Finally two types of source-like contributions can be identified in the equations: the terms $\mathbf{M}_g$, $H_{g\xi}$ and $\mathbf{F}_g$ that represent the transfer of momentum, species and heat through the interface and similar transfer terms that are related to the transfer of mass between the phases.

The averaged equation of state reads

$$\bar{p}_g = R^0 <\rho_g\sum_\xi\frac{Y_\xi}{W_\xi}T_g> \tag{40}$$

Note that for a single component gas this equation gives $\bar{p}_g = \bar{\rho}_g R^0 \tilde{T}_g / W$ and would not require closure.

All the terms discussed are so far unknown and closure relations need to be provided to obtain a solvable system of equations. Closure of the gas phase equations will be discussed in a forthcoming section.

2.4 Derivation and closure of the moment equations for the solid phases

2.4.1 Introduction

The particle averages were defined in an earlier section. In this section we derive the moment equations describing the particles in a macroscopic sense. The derivation given below strongly resembles that used in the kinetic theory of dense gases. In particular, the starting point will be two coupled Boltzmann equations describing the evolution of the single-particle distribution functions, $f_i^{(1)}$, for each particle class i. A distinction from 'ordinary' kinetic theory is that the particles are suspended in a gas, whereas molecules of a gas have only the interaction with other molecules. The influence of the 'interstitial' gas enters the Boltzmann equations and consequently gives rise to terms in the moment equations describing the coupling between particles and gas in a macroscopic way. The separate Boltzmann evolution equations are coupled through the collisions that take place between the particles of the separate particle classes. If these were absent (or negligible as they are in the very dilute limit), the Boltzmann equations would decouple as the effect of the interstitial gas would become dominant. Again, this is a major difference with molecular kinetic theory.

The final difference between the two systems is the inelasticity of the collisions in the gas-particle system. Consequently, as already mentioned in the introduction, the particle fluctuations can not be sustained without a supply of energy from some source (usually from the main flow through mean shear).

Here we discuss a binary mixture of particles suspended in a turbulent carrier gas. Binary granular mixtures have been extensively studied in literature (e.g. Farell et al., 1986; Tham and Gubbins, 1971). However, none of these studies deal with the effects of an interstitial gas. Related to this, all models ultimately assume the granular temperature to be the same for each particle class. This assumption is acceptable when the mass ratio of the particle classes is not too high and there are no 'external' influences on the particle that may regulate the particles temperature.

The present situation is more complex. In dilute situations, the granular temperatures of the particles may be quite different as they react to carrier-phase turbulent fluctuations, and collisions are not frequent enough to equilibrate them. Therefore, below we generalize the analysis by using distinct granular temperatures for each class of particles. Another aspect shared by all papers on binary granular mixtures is that *mixture* equations are derived. Our interest is in deriving *separate* moment equations for each class.

The next section describes the derivation of the moment equations from the Boltzmann equation. The collision dynamics and the particle dynamics are discussed in subsequent sections. Finally, closure is considered.

2.4.2 The transport theorem

The distribution functions for each class are given by solutions of separate Boltzmann equations (Jenkins and Mancini, 1987)

$$\frac{\partial f_i^{(1)}}{\partial t} + \frac{\partial}{\partial \mathbf{x}}[\mathbf{c}_i f_i^{(1)}] + \frac{\partial}{\partial \mathbf{c}_i}[\frac{d\mathbf{c}_i}{dt} f_i^{(1)}] + \frac{\partial}{\partial m_i}[\frac{dm_i}{dt} f_i^{(1)}] + \frac{\partial}{\partial T_i}[\frac{dT_i}{dt} f_i^{(1)}] + \sum_{\xi} \frac{\partial}{\partial Y_{i,\xi}}[\frac{dY_{i\xi}}{dt} f_i^{(1)}] = \sum_{k=A,B} G^{ik} \tag{41}$$

Here, the time-derivatives are to be taken along the particle trajectory. The right hand side of each of these equations denotes the rate of change of the distribution functions due to particle collisions, both with particle belonging to the same class and with other particles as well. It should be understood that the term representing the presence of species is only present for the biomass. Recall the mass weighted ensemble particle average

$$\widetilde{\Psi}_k(\mathbf{x}, t) = \frac{1}{\alpha_k \overline{\rho}_k} \int m_k \Psi_k f_k d\mathcal{Z}^p \tag{42}$$

This average will also be denoted with brackets, i.e.$< \Psi >= \widetilde{\Psi}_k$, which is easier for notation. Multiplying the Boltzmann equation by $m_i\Psi$ and integrating over phase space leads to a dense transport theorem that holds for a generic variable Ψ_i pertaining to class i

$$\frac{\partial \alpha_i \overline{\rho}_i \widetilde{\Psi}_i}{\partial t} + \nabla \cdot \alpha_i \overline{\rho}_i \widetilde{\mathbf{w}}_i \widetilde{\Psi}_i = \sum_{k=A,B} C_{ik}(m_i \Psi_i) - \nabla \cdot \alpha_i \overline{\rho}_i < \mathbf{w}_i' \Psi_i' > + \tag{43}$$

$$\alpha_i \overline{\rho}_i < \frac{d\mathbf{w}_i}{dt} \frac{\partial \Psi_i}{\partial \mathbf{w}_i} > + \alpha_i \overline{\rho}_i < \frac{dT_i}{dt} \frac{\partial \Psi_i}{\partial T_i} > + \tag{44}$$

$$\alpha_i \overline{\rho}_i \sum_{\xi} < \frac{dy_{i\xi}}{dt} \frac{\partial \Psi_i}{\partial y_{i\xi}} > + \alpha_i \overline{\rho}_i < \frac{dm_i}{dt} [\frac{\partial \Psi_i}{\partial m_i} + \frac{\Psi_i}{m_i}] > \tag{45}$$

where the convective part has been decomposed in an average and a Reynolds-like flux term. $C_i(m_i\Psi_i)$ is the mean collisional rate of change of particle property Ψ_i. It represents an integral over all possible (binary) collisions of the change in $m_i\Psi_i$ multiplied by the probability that such a collision occurs. Jenkins and Mancini (1987, 1989) show that this integral can be written as the sum of a source-like contribution and a flux term, representing transport by collisions:

$$C_{ik}(\Psi_i) = \chi_{ik}(\Psi_i) - \nabla \cdot \theta_{ik}(\Psi_i) \tag{46}$$

The precise forms of the collisional integrals for general mixtures that have been given by Jenkins and Mancini (1987, 1989) are very complex and are generalizations of the ones used for single class systems. The moment equations are now easily derived by identifying the generic variable Ψ with a specific choice. Important to note at this point is that the moment equations equations can only be written when the collision dynamics and the particle dynamics along its motion are both specified. These two subjects are discussed subsequently.

2.4.3 Collision dynamics

It is assumed that only binary collisions take place, i.e. collisions between multiple particles are neglected. Although at high solids concentrations this is questionable (especially when the particle size ratio is large), it is the only mathematically tractable approach (even in the simpler, molecular theory; see Chapman and Cowling, 1970).

After Jenkins and Mancini (1987), we consider two particle classes, A and B. These particles are assumed perfectly smooth and spherical. Their respective masses and diameters are m_A, m_B,

σ_A, and σ_B. Consider a collision between particle 1 of class i and particle 2 of class k where i and k may be A or B. Furthermore, primes will be used to denote a variable right after collision, a variable without a prime denoting a variable right before collision; this notation is used throughout. Below we consider the conservation of momentum and energy (mass and species are trivial) during a collision between particle 1 and 2.

Momentum The relation between the velocities of the particles right before and after a collision can be determined from the conservation of momentum and (mechanical) energy. Define the relative velocities $\mathbf{c}_{21}$ and $\mathbf{c}'_{21}$ as

$$\mathbf{c}_{21} = \mathbf{c}_2 - \mathbf{c}_1 \tag{47}$$
$$\mathbf{c}'_{21} = \mathbf{c}'_2 - \mathbf{c}'_1 \tag{48}$$

Let $\mathbf{k}$ be the unit vector directed from the center of particle 2 to the center of particle 1 at collision. Then the components of the relative velocities in the direction of $\mathbf{k}$ before and after collision are assumed to be related by

$$\mathbf{k} \cdot \mathbf{c}'_{21} = -e_{ik}(\mathbf{k} \cdot \mathbf{c}_{21}) \tag{49}$$

where e_{ik} is the restitution coefficient for a collision between a particle i and k (note: $e_{ik} = e_{ki}$). Further define $m_{ik} = m_i + m_k$ and $M_i = m_i/m_{ik}$. The center of mass velocity $\mathbf{G}_{ik}$ is constant during a collision and equals

$$\mathbf{G}_{ik} = M_k\mathbf{c}_2 + M_i\mathbf{c}_1 = M_k\mathbf{c}'_2 + M_i\mathbf{c}'_1 \tag{50}$$

Finally, we have

$$\mathbf{c}'_1 - \mathbf{c}_1 = M_k(1 + e_{ik})(\mathbf{k} \cdot \mathbf{c}_{21})\mathbf{k} \tag{51}$$
$$\mathbf{c}'_2 - \mathbf{c}_2 = -M_i(1 + e_{ik})(\mathbf{k} \cdot \mathbf{c}_{21})\mathbf{k} \tag{52}$$

Now in general for any particle property $\Psi = \Psi(\mathbf{c})$ these relations may be used to calculate its rate of change $\Psi' - \Psi$ in a collision.

Heat At the onset of this section we have assumed collisions to be binary and instantaneous. As a result, the heat exchange between particles during a collision vanishes. This is however not realistic. A true collision (or more accurate; an interaction) will be somewhere between a collision and a sliding contact. We will characterize an interaction between two particles by a contact area A_c and a contact time τ_c. The heat transfer during this contact is readily estimated by the model of two uniform one-dimensional, semi-infinite slabs at temperatures T_1 and T_2, conductivity λ_1 and λ_2, and heat capacities C_{p1} and C_{p2}. The heat exchange during this contact then equals

$$\Delta E = 2A_c\sqrt{\tau_c/\pi}\left(\frac{\omega_1\omega_2}{\omega_1 + \omega_2}\right)(T_1 - T_2) \tag{53}$$

where $\omega_i = \sqrt{\rho_i C_{pi}\lambda_i}$. This analysis is valid for short contact times only, as it is based on penetration theory. The contact area is mainly determined by the smallest particle (having radius r_s). The area is estimated as the surface area spanned by a solid contact angle Ω_c of order one:

$$A_c = \Omega_c r_s^2 \tag{54}$$

The contact time is further estimated

$$\tau_c = K_c\frac{r_s}{|\mathbf{c}_2 - \mathbf{c}_1|} \tag{55}$$

where K_c is an empirical parameter to be determined from comparisions of simulations with detailed experimental data. The rationale for the above choice is that the time available for contact decreases as the relative velocity increases.

2.4.4 Particle dynamics

The second component needed for the derivation of the moment equations is the rate of change of the particle properties along their trajectory.

Species As outlined earlier, the biomass kinetics behaves volumetrically, i.e. the mass conversion rates are linear in the mass of the particle itself. In general we may write

$$\frac{dm_\xi}{dt} = \frac{dmY_\xi}{dt} = mR_\xi \tag{56}$$

where R_ξ represents the total rate, and may be the sum of several reactions involving the same component. As an example, the rate R for the one of the active solids species is

$$R_{active} = -Y_{active}(K_2 + K_3) \tag{57}$$

The rate depends (linearly) on the mass fractions and nonlinear on the particle temperature. From the previous equation one obtains the rate of change of Y_ξ

$$\frac{dY_\xi}{dt} = R_\xi - \frac{Y_\xi}{m}\frac{dm}{dt} \tag{58}$$

Mass The rate of change of the particle mass is obtained by summing the individual species rates

$$\frac{dm}{dt} = \sum_\xi \frac{dm_\xi}{dt} = m\sum_\xi R_\xi \tag{59}$$

In practice, only some reactions contribute to phase change. In the present case, only reactions K_2 and K_3 need to be considered.

Momentum The rate of change of the velocity of a single particle in a gas can be written as

$$m\frac{d\mathbf{w}}{dt} = \mathbf{F}^p = m\mathbf{g} - V_p\nabla\overleftarrow{p}_g + \mathbf{F}_r \tag{60}$$

The terms on the right hand side denote the gravitational body force, the force due to the gas pressure gradient and the drag force. The drag force can be written in the general form $\mathbf{F}_r = -\rho_g(\pi d^2/8)C_d|\mathbf{u}_r|\mathbf{u}_r$ with $\mathbf{u}_r = \mathbf{w} - \overleftarrow{\mathbf{u}}_g$; $\overleftarrow{\mathbf{u}}_g$ and $\overleftarrow{p}_g$ are the velocity and gas pressure of the locally undisturbed fluid flow at the position of the particle center. In the dilute regime, the drag coefficient is determined from the correlation $C_d = 24/\,\mathrm{Re}_p(1 + 0.15\,\mathrm{Re}^{0.687})$ whereas in the dense regime, an Ergun relation is used. Note that C_d may be corrected for the blowing of the particle as in the validated model of Miller et al. (1998b).

Energy The rate of change of the particle's internal energy is due to heat exchange with the surrounding gas, heat of reaction and loss of vapor components:

$$\frac{d(mh)}{dt} = Q_r + Q_{\Delta h} + \frac{dm}{dt} h_v \tag{61}$$

where h and h_v denote the average enthalpies of the particle and vapors exiting the particle, respectively. The combined effect of convective and conductive heat transfer can be written as

$$Q_r = -\lambda_g \pi d_{eff} \mathrm{Nu}(\mathrm{Re}, \mathrm{Pr})(T - \overleftrightarrow{T}_g) \tag{62}$$

where the appropriate Nusselt relation depends on the operating parameters (slip velocity etc.). The introduction of the effective particle diameter, d_{eff}, is a way to correct for the porosity of the biomass particles. For the sand, the last two terms in the balance equation are absent.

2.4.5 The moment equations

By making specific choices for the general variable Ψ in the transport theorem, specific moment equations are recovered.

Mass The mass conservation equations are recovered by taking $\Psi = 1$:

$$\frac{\partial(\alpha\overline{\rho})_i}{\partial t} + \nabla \cdot (\alpha\overline{\rho}\widetilde{\mathbf{w}})_i = \Gamma_i \tag{63}$$

where the mass transfer $\Gamma_i = \alpha_i\overline{\rho_i} < \frac{1}{m_i}\frac{dm_i}{dt} >= \alpha_i\overline{\rho_i}\sum_\xi < R_\xi >$ can be coupled to the conversion rate of solid- to gas-phase reactions. For the sand, this term is absent.

Momentum The momentum equations are generated using $\Psi = \mathbf{w}$

$$\begin{aligned} \frac{\partial \alpha_i\overline{\rho_i}\widetilde{\mathbf{w}}_i}{\partial t} + \nabla \cdot \alpha_i\overline{\rho}_i\widetilde{\mathbf{w}}_i\widetilde{\mathbf{w}}_i &= \alpha_i\overline{\rho}_i < \frac{\mathbf{F}_i^p}{m_i} > + \alpha_i\overline{\rho}_i < \frac{dm_i}{dt}\frac{\mathbf{w}_i}{m_i} > \\ &\quad -\nabla \cdot \mathbf{\Sigma}_i + \sum_{k=A,B} \chi_{ik}(m_i\mathbf{w}_i) \end{aligned} \tag{64}$$

where $\mathbf{\Sigma}_i = \alpha_i\overline{\rho}_i < \mathbf{w}_i'\mathbf{w}_i' > + \sum_{k=A,B} \theta_{ik}(m_i\mathbf{w}_i)$. The first term on the right hand side is the average force exerted on the particle by the surrounding gas; the second represents the effect of mass transfer. The effective stress tensor $\mathbf{\Sigma}_i$ consists of a kinetic part and a collisional part which incorporates both effects from collisions between particles of the same class and between unlike particles. The final term in the transport equation is a source term which is also composed of collisional contributions between like and unlike particles. However, as total linear momentum of phase i is conserved in a collision between two particles of that phase, only unlike particle collisions contribute to this term. Note that an equivalent term does not appear in single-class systems.

Species Taking $\Psi = Y_\xi$ gives

$$\frac{\partial \alpha_i\overline{\rho}_i\widetilde{Y}_{i\xi}}{\partial t} + \nabla \cdot \alpha_i\overline{\rho}_i\widetilde{\mathbf{w}}_i\widetilde{Y}_{i\xi} = -\nabla \cdot \alpha_i\overline{\rho}_i < \mathbf{w}_i'Y_{i\xi}' > + \Gamma_{i\xi} \tag{65}$$

The first term on the right hand side denotes the turbulent transport of the mass fraction. The second term, $\Gamma_{i\xi} = \alpha_i\overline{\rho}_i < R_\xi >$ is the average mass source arising from reaction. Note that no collisional terms are present as the mass fractions do not change during a collision.

Granular temperature When the general variable Ψ is a function of the fluctuating velocity rather than the actual velocity, the transport theorem needs to be rederived (Jenkins and Richman, 1987; Chapman and Cowling, 1970). Doing so and applying the same procedure as used for the other moments to the variable $\Psi = 1/2w_i'^2$ one obtains

$$\begin{aligned}\frac{3}{2}[\frac{\partial \alpha_i \overline{\rho}_i \Theta_i}{\partial t} + \nabla \cdot \alpha_i \overline{\rho}_i \widetilde{\mathbf{w}}_i \Theta_i] &= -\mathbf{\Sigma}_i : \nabla \widetilde{\mathbf{w}}_i - \nabla \cdot \mathbf{q}_i \\ + \sum_{k=A,B} \chi_{ik}(\frac{1}{2} m_i w_i'^2) + \alpha_i \overline{\rho}_i &< \frac{dm_i}{dt} \frac{1/2 w_i'^2}{m_i} > + \alpha_i \overline{\rho}_i < \frac{\mathbf{F}_i^p}{m_i} \cdot \mathbf{w}_i' > \end{aligned} \tag{66}$$

where $\Theta_i = 1/3 w_i'^2$ is the granular temperature and $\mathbf{q}_i = \alpha_i \overline{\rho}_i < 1/2 w_i'^2 \mathbf{w}_i' > + \sum_{k=A,B} \theta_{ik}(1/2 m_i w_i'^2)$. The first term on the right hand side is the production of fluctuational kinetic energy due to shearing of the solid phase this mechanism being identical to that found in single-phase turbulence. The mechanical energy balance of the particle mean motion contains this term with the opposite sign expressing an exchange mechanism. The next term denotes the flux of fluctuational energy due to velocity fluctuations themselves (kinetic part) and due to collisions (again containing contributions from both like and unlike particles). Similar to the momentum equation, the source term is composed of a sum over both particle classes. Here, however, due to the inelasticity of collisions, both parts indeed contribute. The effect of mass transfer is contained in the forelast term. The final term represents the coupling with the surrounding gas phase.

Heat Choosing $\Psi = h$, one obtains

$$\begin{aligned}\alpha_i \overline{\rho}_i \frac{D\widetilde{h}_i}{Dt} &= \alpha_i \overline{\rho}_i [< \frac{Q_{r,i}}{m_i} > + < \frac{Q_{\Delta h,i}}{m_i} >] + \alpha_i \overline{\rho}_i < \frac{dm_i}{dt} \frac{h_v}{m_i} > - \Gamma_i \widetilde{h}_i \\ &\quad -\nabla \cdot \alpha_i \overline{\rho}_i < \mathbf{w}_i' h_i' > - \sum_{k=A,B} \nabla \cdot \theta_{ik}(m_i h_i) + \sum_{k=A,B} \chi_{ik}(m_i h_i) \end{aligned} \tag{67}$$

Here, the terms on the right hand side denote the mean heat transfer with the surrounding gas, the heats of reaction, the mean enthalpy of the vapors exiting the porous particle, a mass transfer term resulting from the non-conservative form of the equation, the 'turbulent' flux and the collisional contributions. The source-like term χ only contributes through collisions between unlike particles.

2.4.6 Closure

The above system of equations contains several correlations and is therefore unclosed. Several types of correlations may be distinguished: (i) Mass transfer (reaction) related correlations. (ii) Kinetic contributions to transport processes (Reynolds terms). (iii) Collisional contributions to both transport and source terms. (iv) Interactions with the surrounding gas.

In principle, all correlations could be computed from the single particle velocity distribution (except for the collisional integrals which require knowledge of the complete pair distribution function, and the gas-particle interaction which requires a joint probability distribution function of the gas and particles phases). The single particle distribution functions are solutions of the Boltzmann equations given earlier. These solutions are too complex to derive when the phase space includes so many variables (mass fractions, temperature, etc.). Therefore, the distributions (and the Boltzmann equations) are reduced to include only the distribution of velocities.

In the present paper, a further simplification is made. Instead of using a distribution as computed from the Boltzmann equations, a Maxwellian distribution is assumed, i.e. the lowest order approximation to the Boltzmann equation:

$$f_i^{(1)}(\mathbf{x}, \mathbf{c}_i, t) = \frac{n_i}{(2\pi\Theta_i)^{3/2}} \exp[\frac{-(\mathbf{c}_i - \widetilde{\mathbf{w}}_i)^2}{2\Theta_i}] \tag{68}$$

This is a good approximation when the flow has small spatial gradients, the collisions are nearly elastic and the particles are heavy enough (as measured by the turbulence time scales being much smaller than the particle relaxation time, i.e. the particle-fluid correlation is small).

The mass exchange terms in the mass and species equations are evaluated at the average temperature and mass fractions, i.e.

$$\Gamma_i = \alpha_i \overline{\rho}_i \sum_\xi < R_\xi >= \alpha_i \overline{\rho}_i \sum_\xi R_\xi(\widetilde{Y}, \widetilde{T}) \tag{69}$$

and a similar expression for the species mass sources. This procedure neglects correlations between temperature and the mass fractions. As the species equations are of first order, these approximations are not too strict. A comparable approach, using mean values of temperature, is used for the evaluation of the heat of reaction and the average enthalpy flux of the vapor products.

The momentum and granular temperature equations also contain mass transfer related terms. They have the general form

$$\alpha_i \overline{\rho}_i < \frac{dm_i}{dt} \frac{\phi_i}{m_i} > \tag{70}$$

where ϕ is the particle property of interest. These correlations are modeled as

$$\alpha_i \overline{\rho}_i < \frac{dm_i}{dt} \frac{\phi_i}{m_i} > \approx \alpha_i \overline{\rho}_i \Gamma_i \widetilde{\phi}_i \tag{71}$$

Two types of kinetic stresses are present in the equations; those depending on the velocities only and those that also depend on some other variable, e.g. $< \mathbf{w}' Y_\xi' >$. The first are readily calculated from the Maxwellian distributions. The second type has to be modeled since the distribution of the transported variable is not available. The approach followed here is that taken by Louge et al., (1993). Using elementary kinetic theory, the kinetic transport terms may be written as diffusion fluxes, e.g.

$$-\nabla \cdot \alpha_i \overline{\rho}_i < \mathbf{w}_i' Y_{i\xi}' >= \nabla \cdot \alpha_i \overline{\rho}_i D_{ii} \nabla \widetilde{Y}_{i\xi} \tag{72}$$

where D_{ii} is the self diffusion coefficient of particle class i. This coefficient may be calculated from the Maxwellian distribution (see Chapman and Cowling, 1970). A similar relation holds for the enegy equation.

The collisional contributions are dependent on the complete pair distribution function defining the probability that two particles have certain positions and velocities. This pair distribution is then expressed as the product of the single particle distribution of each particle with a factor that incorporates the effect of the excluded volume. The collisional contributions may then be calculated. The results of these computations are similar to those given by Jenkins and Mancini (1987).

The final class of correlations concerns those containing the effects of the interstitial gas. Both the momentum, energy and granular temperature equations contain terms that reflect interaction with the carrier gas. The interaction term in the momentum equation may be expanded to read

$$\alpha_i \overline{\rho}_i < \frac{\mathbf{F}_i^p}{m_i} >= \alpha_i \overline{\rho}_i [\mathbf{g} - < \frac{V_p}{m_i} \nabla \overleftrightarrow{p}_g > - < \frac{1}{\tau_{12}} (\mathbf{w}_i - \overleftrightarrow{\mathbf{u}}_g) >] \tag{73}$$

where τ_{12} ($= \rho_p d_p^2/18\mu_g$ for Stokes drag) represents the particle relaxation time. The pressure gradient term is usually closed in terms of the mean gas pressure gradient:

$$-\alpha_i \overline{\rho}_i < \frac{V_p}{m_i} \nabla \overleftarrow{p}_g > \approx -\alpha_i \nabla \overline{p}_g \tag{74}$$

Similarly, for the drag force related term:

$$-\alpha_i \overline{\rho}_i < \frac{1}{\tau_{12}} (\mathbf{w}_i - \overleftarrow{\mathbf{u}}_g) > \approx -\frac{\alpha_i \overline{\rho}_i}{\tau_{12}} (\widetilde{\mathbf{w}}_i - < \overleftarrow{\mathbf{u}}_g >) \tag{75}$$

where fluctuations in the particle relaxation time are neglected. The particle average of the locally undisturbed velocity is usually set equal to the phase averaged velocity: $< \overleftarrow{\mathbf{u}}_g > \approx \widetilde{\mathbf{u}}_g$. A similar procedure is followed for the interaction term in the granular temperature equation:

$$\alpha_i \overline{\rho}_i < \frac{\mathbf{F}_i^p}{m_i} \cdot \mathbf{w}_i' > = \frac{\alpha_i \overline{\rho}_i}{\tau_{12}} (< \mathbf{w}_i' \cdot \mathbf{u}_g'' > - < \mathbf{w}_i' \cdot \mathbf{w}_i' >) \tag{76}$$

where we have decomposed the undisturbed gas velocity as $\overleftarrow{\mathbf{u}}_g = < \overleftarrow{\mathbf{u}}_g > + \mathbf{u}_g''$. Note that all of the above averages are particle averages. The first term on the right hand side is the fluid-particle correlation and may be either positive or negative; the second term is inherently negative and reduces the granular temperature due to particle drag. For heavy particles the first term is small and may be neglected. The end result is

$$\alpha_i \overline{\rho}_i < \frac{\mathbf{F}_i^p}{m_i} \cdot \mathbf{w}_i' > \approx \frac{\alpha_i \overline{\rho}_i}{\tau_{12}} (-3\Theta_i) \tag{77}$$

The energy equation contains the interaction term $\alpha_i \rho_i < Q_{r,i} >$ that accounts for the gas-particle heat transfer. The following closure is provided for this term

$$\alpha_i \rho_i < \frac{Q_{r,i}}{m_i} > = -\frac{6\alpha_i \lambda_g}{d_{eff}^2} < \mathrm{Nu} > (\widetilde{T}_i - \widetilde{T}_g) \tag{78}$$

where the average Nusselt number is calculated from the mean slip velocity, etc. For low turbulence intensity of the gas and solids (compared to the average slip velocity), this is an accurate approximation. Note that Louge et al. (1993) have incorporated the effect of particle velocity fluctuations on the Nusselt number. In view of the complexity of the overall problem, such an approach has not been pursued here.

2.5 Closure of the gas phase transport equations and the modeling of turbulence

The gas phase macroscopic equations derived previously contain correlations that need to be expressed in terms of the average variables in order to obtain a solvable system. When phase ensemble averages are taken for both phases, it is customary to write jump conditions which lead after averaging to relations between interfacial coupling terms in the macroscopic equations. Here, ensemble particle averages are used for the particulate phase where the particles are described in terms of global parameters. Hence, no local jumpconditions can be defined. Integral conservation relations can however be specified. More specifically, the standard local jump conditions are integrated over the surface of the particle and the contribution from the particle side of the interface is replaced by the rate of change of a particle property.

In this section, we start with a discussion of the closure relations for the momentum equations, except for the Reynolds stresses. These are the subject of the next section. The subsequent sections discuss closure of the energy and species equations.

2.5.1 Mass

The mass transfer rate, Γ_g is related to the solid to gas reactions of the biomass particle (tar production). Closure of the similar term in the biomass equation was already outlined. It is consistent to use $\Gamma_g = -\Gamma_b$.

2.5.2 Momentum

The momentum equations contain four unknown correlations, a molecular and a turbulent stress, interfacial coupling and a mass transfer related term. The turbulent Reynolds stress is discussed in a separate section. The mass transfer related term is easily approximated as

$$\Gamma_g \widehat{\mathbf{u}}_g^i = \Gamma_g \widetilde{\mathbf{u}}_b \tag{79}$$

Hence, the average interfacial gas velocity is approximated by the biomass velocity.

The molecular stress and interfacial coupling are discussed together. Following Drew (1983), the momentum transfer term may be decomposed into two contributions:

$$\mathbf{M}_g = -p_g^i \nabla \alpha_g + \mathbf{M}_g' \tag{80}$$

where the first term is called the buoyant force and accounts for the effect of the average interfacial pressure distribution, and $M_g' =< (p_g - p_g^i)\nabla\chi_g - \boldsymbol{\tau}_g \cdot \nabla\chi_g >$ denotes the remainder of the momentum interaction. The objective of this splitting is to incorporate, to first order, the effect of non-homogeneity of the mixture. The momentum equation is now

$$\frac{\partial(\alpha\overline{\rho}\mathbf{u})_g}{\partial t} + \nabla\cdot(\alpha\overline{\rho}\widetilde{\mathbf{u}}\widetilde{\mathbf{u}})_g = -\alpha_g\nabla\overline{p}_g + \nabla\cdot[\alpha\overline{\boldsymbol{\tau}} + \boldsymbol{\Sigma}^{\mathrm{Re}}]_g + \alpha_g\overline{\rho}_g\mathbf{g} + \mathbf{M}_g' + \Gamma_g\widehat{\mathbf{u}}_g^i \tag{81}$$

where the difference between the averaged gas pressure and the average interfacial pressure has been neglected. The phase averaged viscous stress is now approximated by a form similar to its microscopic counterpart

$$\overline{\tau}_g = \mu[(\nabla\widetilde{\mathbf{u}}_g) + (\nabla\widetilde{\mathbf{u}}_g)^{\mathrm{T}} - 2/3(\nabla\cdot\widetilde{\mathbf{u}}_g)] \tag{82}$$

The interfacial transfer term consists mainly of drag in gas-particle flows and the expression is taken to be the sum of the expressions used in the averaged solid momentum equations.

2.5.3 Turbulence transport modeling

Second order closure models constitute the highest possible level of closure currently feasible in terms of computational effort. On the other hand, two-equation models represent the minimum acceptable level of closure that specify an internal length scale. All of the models presented in literature for fluidized beds use a $k-\varepsilon$ based gas phase turbulence model (or none at all). It has been argued (Balzer, 1993) that the precise turbulence model is not very critical in the dense regions of the bed as the particle motion is completely dominated by collisions. In the present application however, it is important to have an accurate prediction of heat transfer processes and hence to have an accurate turbulence model. The gas phase turbulence model is also important in the prediction of the recirculating gas flow pattern in and around the 'bubbles' (Balzer, 1993) in the fluidized bed which in turn may have effects on the thermal and reactive behavior of the bed.

The transport equations for the Reynolds stress tensor can be derived by considering the following ensemble average $< \chi_g \mathbf{u}_i' N(\mathbf{u}_j) + \chi_g \mathbf{u}_j' N(\mathbf{u}_i) >$. Here, $N(\mathbf{u}_i)$ represents the Navier Stokes

operator. After much tedious manipulation one obtains

$$\frac{\partial \alpha\bar{\rho}\widetilde{R}_{ij}}{\partial t} + \frac{\partial \alpha\bar{\rho}\widetilde{u}_k\widetilde{R}_{ij}}{\partial x_k} = P_{ij} + T_{ij} + \Pi_{ij} + \varepsilon_{ij} + W_{ij} + \Gamma_g\widehat{R}^i_{ij} \tag{83}$$

where all phase indices have been omitted for clarity. The terms on the right hand side are abbreviations of the following averages

$$\begin{aligned}
P_{ij} &= -\alpha\rho[\widetilde{R}_{ik}\frac{\partial u_j}{\partial x_k} + \widetilde{R}_{jk}\frac{\partial u_i}{\partial x_k}] \\
T_{ij} &= \frac{\partial}{\partial x_k}\alpha[\overline{-\rho u_i' u_j' u_k' + u_i'\sigma_{jk} + u_j'\sigma_{ik}}] \\
\Pi_{ij} &= \alpha[\overline{p'\frac{\partial u_i'}{\partial x_j} + p'\frac{\partial u_j'}{\partial x_i}}] \\
\varepsilon_{ij} &= -\alpha[\overline{\tau_{ik}'\frac{\partial u_j'}{\partial x_k} + \tau_{jk}'\frac{\partial u_i'}{\partial x_k}}] \\
W_{ij} &= -<\sigma_{jl}u_i'\frac{\partial \chi_g}{\partial x_l} + \sigma_{il}u_j'\frac{\partial \chi_g}{\partial x_l}> \\
\Gamma_g\widehat{R}^i_{ij} &= <\rho u_i' u_j'(u_l - u_{li})\frac{\partial \chi_g}{\partial x_l}>
\end{aligned}$$

Here, P_{ij} represent production due to mean shear; note that this term does not need closure. T_{ij} denotes the turbulent transport due to velocity fluctuations. Π_{ij} is the pressure-strain correlation responsible for redistribution of energy among the various components. Viscous dissipation is incorporated through ε_{ij}. The term W_{ij} is an interfacial average and represents the production or dissipation due to interfacial work. Finally, the last term accounts for the effect of mass transfer between phases. All terms in this equations except for the last two contributions have counterparts in single-phase flows. It is therefore not surprising that the modelling of the correlations is tailored after the single-phase flow case. The modeling of these terms is discussed below.

The most popular model for turbulent transport is the Generalized Gradient Diffusion Hypothesis (GGDH) by Daly and Harlow (1970). In this model turbulent transport is expressed in terms of the gradient of the stress tensor. Due to its form, it is able to describe counter gradient diffusion. A drawback however is its violation of invariance. Extended to compressible multiphase flow, the GGDH reads

$$T_{ij} = \frac{\partial}{\partial x_k}[\alpha(C_\varepsilon\bar{\rho}\frac{\widetilde{k}}{\varepsilon}\widetilde{R}_{kl} + \mu_g)]\frac{\partial \widetilde{R}_{ij}}{\partial x_l} \tag{84}$$

At high enough Reynolds numbers the small scale turbulence is in local equilibrium, having isotropic dissipation. This is the most common assumption used in stress transport models. Here, it is assumed that the presence of the particles does not affect this local equilibrium too much, i.e. isotropy is still assumed:

$$\varepsilon_{ij} = \frac{1}{2}\varepsilon_{ll}\delta_{ij} = -\frac{2}{3}\alpha\bar{\rho}\varepsilon \tag{85}$$

This is consistent with the experimental result that particle laden flows have an energy spectrum that exhibits the same power dependence (-5/3) as single-phase flows. The pressure strain correlation is a redistribution term, i.e. it is traceless, $\Pi_{ll} = 0$. Having the same order of magnitude as the production terms, it plays an important role in accurate prediction of stress anisotropy. Most

efforts of modelers have traditionally been directed towards this term. As a result many models are available in literature. Here we propose to use a model by Zha and Knight (1996) that has proven successful in the description the vortex reactor (Miller and Bellan, 1998). Extension of this model to the multifluid case results in

$$\Pi_{ij} = -C_{p1}\alpha\bar{\rho}\frac{\varepsilon}{k}[\widetilde{R}_{ij} - \frac{2}{3}\widetilde{k}\delta_{ij}] + C_{p2}\alpha\bar{\rho}\widetilde{k}(\frac{\partial\widetilde{u}_i}{\partial x_j} + \frac{\partial\widetilde{u}_j}{\partial x_i}) \tag{86}$$

An alternative expression may be the 'standard model' (Gibson and Launder, 1978). The 'standard model', however is more complex to implement than the above compressible form.

The interfacial work term is repeated here for convenience:

$$W_{ij} = - < \sigma_{jk}u_i'\frac{\partial\chi_g}{\partial x_l} + \sigma_{ik}u_j'\frac{\partial\chi_g}{\partial x_l} > \tag{87}$$

This interfacial average can be rewritten as a series of particle averages of which the first term states

$$W_{ij} = n\overline{[u_i'\int dS_l\sigma_{jl} + u_j'\int dS_l\sigma_{il}]} \tag{88}$$

where the overbar indicates particle averaging and where the velocity fluctuations have been taken outside the surface integrals. This final manipulation is possible when the particles are nonrotating, i.e. in that case the velocity of their surface is essentially constant. Now note that these surface integrals are the components of the force exerted on the particle, i.e.

$$W_{ij} = n\overline{[u_i'F_j + u_j'F_i]} \tag{89}$$

Using the fact that the drag force constitutes the primary force on the particle we finally obtain

$$W_{ij} = \sum_{k=s,b}\frac{\alpha_k\rho_k}{\tau_{k,12}}[-2\overline{u_{gi}'u_{gj}'} + \overline{u_{gi}'w_{kj}'} + \overline{u_{gj}'w_{ki}'}] \tag{90}$$

The sum extends over the sand and biomass particles. For heavy particles, the last two terms expressing fluid-particle correlations are small compared to the first term. Retaining only the first term and assuming that this particle average is equal to the gas phase ensemble average we obtain the final result, a dissipative term

$$W_{ij} = \sum_{k=s,b} -2\frac{\alpha_k\rho_k}{\tau_{k,12}}\widetilde{R}_{ij} \tag{91}$$

In the case of isotropic modelling, contraction of the above expression reduces to that used by Louge and Jenkins (1993) and Bolio and Sinclair (1995).

The mass transfer related interfacial term will be modeled when we have more insight into the problem as brought by simulations of simplified situations.

In addition to closure of the unknown correlations in the stress equations, a transport equation needs to be supplied for the dissipation rate ε. Although such a derivation is feasible using a similar derivation as above, this equation would contain a large number of correlations. Therefore, usually, a more heuristic approach is taken and a transport equation is borrowed from incompressible single phase flows and expanded to include the effect of the interfacial transfer. The equation proposed here is

$$\frac{\partial\alpha\bar{\rho}\varepsilon}{\partial t} + \frac{\partial\alpha\bar{\rho}\widetilde{u}_k\varepsilon}{\partial x_k} = \frac{\partial}{\partial x_k}[\alpha(C_\varepsilon\bar{\rho}\frac{\widetilde{k}}{\varepsilon}\widetilde{R}_{kl} + \mu_g)]\frac{\partial\varepsilon}{\partial x_l} + \frac{\varepsilon}{\widetilde{k}}[C_{\varepsilon 1}P_k - \alpha\bar{\rho}C_{\varepsilon 2}\varepsilon] + C_{\varepsilon 3}\frac{\varepsilon}{\widetilde{k}}W_k \tag{92}$$

where the right hand side of the equation consists of production and dissipation, turbulent diffusion as modeled by a generalized gradient diffusion hypothesis and the interfacial transfer W_ε.

2.5.4 Species

The species equations contain two unknown flux terms as well as sources resulting from mass transfer and chemical reaction. The molecular and turbulent fluxes are handled similar to the fluxes in the Reynolds stress model described earlier:

$$-\nabla \cdot [\alpha \mathbf{j}_\xi + \mathbf{j}_\xi^{\mathrm{Re}}]_g = \frac{\partial}{\partial x_k} \alpha\rho [C_Y \frac{\widetilde{k}}{\varepsilon} \widetilde{R}_{kl} + D_\xi] \frac{\partial \widetilde{Y}_\xi}{\partial x_l} \tag{93}$$

As far as gas-phase reactions are concerned (tar to gas conversion), these are handled similarly to the biomass, i.e. the average rate of reaction is calculated from the mean mass fractions and temperature:

$$\alpha\overline{\rho}\widetilde{R}_\xi = \alpha\overline{\rho} R_\xi(\widetilde{Y}, \widetilde{T}) \tag{94}$$

As far as interfacial transfer is concerned, these are only relevant for the tar and gas species. The combined terms $H_{g\xi} + \Gamma_g \widehat{Y}_{g\xi}^i$ form a mass source for the species equations originating from solid to gas phase reactions. These are again calculated at the mean temperature and solid mass fractions

$$H_{g\xi} + \Gamma_g \widehat{Y}_{g\xi}^i = \alpha_b \rho_b R_\xi(\widetilde{Y}, \widetilde{T}) \tag{95}$$

2.5.5 Heat

The enthalpy equation contains two unknown fluxes and three source terms. The molecular and turbulent fluxes are modeled together in terms of the gradient of the mean gas temperature:

$$-\nabla \cdot [\alpha \mathbf{q}_\xi + \mathbf{q}_\xi^{\mathrm{Re}}]_g = \frac{\partial}{\partial x_k} \alpha_g \overline{\rho}_g [C_Y C_p \frac{\widetilde{k}}{\varepsilon} \widetilde{R}_{kl} + \lambda_g] \frac{\partial \widetilde{T}_g}{\partial x_l} \tag{96}$$

The mean heat of gas-phase reaction are calculated from the mean reaction rates. This is identical to the procedure used for the reaction terms in the species equations.

For apparent reasons, the surface heat flux, F_g, and the convective heat flux, $\Gamma_g \widehat{h}_g^i$, are set equal to the corresponding terms in the particle equations. Thus, we have

$$F_g = \sum_{i=s,b} \alpha_i \overline{\rho}_i < Q_{r,i}/m_i > \tag{97}$$

$$\Gamma_g \widehat{h}_g^i = \alpha_i \overline{\rho}_i < \frac{dm_b}{dt} \frac{h_v}{m_b} > \tag{98}$$

These equalities are a direct result of the integrated jump conditions mentioned in the introduction of section 2.5.

2.5.6 Equation of state

The averaged equation of state for the gas is written as

$$\overline{p}_g = \overline{\rho}_g R^0 \sum_\xi \frac{\widetilde{Y}_\xi}{W_\xi} \widetilde{T}_g \tag{99}$$

where the correlation between the species mass fractions and temperature are neglected. This is a reasonable assumption since the species concentration fluctuations are expected to be small.

3 Numerical method

Numerical codes that have been used in literature can be broadly divided into two classes. i) Methods based on extension of the SIMPLE algorithm. ii) Methods based on extensions of a code called KFIX (Rivard and Torrey, 1977).

Codes belonging to the first class are usually employ a fully implicit time discretization. In these algorithms, the difference equations are solved in a sequential manner and updated until overall convergence is reached. One of the drawbacks of these algorithms is that it is not obvious how to obtain the pressure and the volume fractions. Usually one of the mass conservation equations is chosen as the candidate for the volume fraction while the other (or the mixture) is taken as the basis for a pressure correction equation. Effects of the solids pressure can also be heuristically accounted for (Syamlal, 1998). Our own experience has shown that (depending on the timestep) between 10 and 20 iterations per timestep are necessary to obtain convergence.

The second class of methods is of a more explicit nature, although all interphase transfer mechanisms are treated implicitly. Here, the gridpoints are visited sequentially and at each of those points an iterative schemes drives the discrete equations at that point to convergence. Even when the iterative scheme at a point is efficient, the overall convergence is dominated by low wavenumber errors which damp very slowly, a situation exceedingly expensive on large grids.

In the present paper, a new algorithm is outlined based on simultaneous solution of the volume fractions (hence, the solids pressure) and the gas pressure. The method can be viewed as an extension of the single-phase pressure correction method to the multifluid case.

3.1 Numerical discretization

The discretization is based on the finite volume method on a two dimensional staggered grid which is the most suitable for the low Mach number flow of interest. As this method is well established the discussion is restricted to the necessary details and deviations from standard procedure.

3.1.1 Spatial discretization

One major weakness of most multifluid discretizations is the appearance of numerical diffusion caused by the use of first order upwind schemes for approximating the convective terms. Its effect is found to be most severe in the mass conservation equations due to the lack of physical diffusion. Numerical diffusion is however also known to plague turbulence and momentum equations, especially when stress transport closures are used. As far as fluidized bed applications are concerned, numerical diffusion leads to unphysical 'bubble' (i.e. regions containing few particles) shapes having a pointy roof instead of the more spherical shape as found in experiments (Syamlal, 1997).

To reduce this effect, all convective terms are approximated using a nonlinear TVD (Total Variation Diminishing) scheme. Cell face values are calculated from an upwind value and a suitable antidiffusive part, their blend being controlled by the local gradients in the solution. We have selected Roe's modified second order upwind scheme combined with the Van Leer flux limiter (see e.g. Hirsch, 1990) because of its good performance in scalar convection problems (see e.g. Tamamidis and and Assanis, 1993). Roe's scheme is second order accurate in smooth regions and reduces locally to first order when the solution is non-smooth.

Besides accuracy, TVD schemes have the favorable property that no new extrema are created in the solution. This is especially important for inherently positive variables, such as turbulence parameters or volume fractions which are bounded between 0 and 1.

3.1.2 Temporal discretization

After spatial discretization, a set of ODE's results that must be integrated in time. The flow of interest is a very low Mach number flow. Hence, the timestep restriction related to the propagation of acoustic modes is much stronger compared to the Courant restriction and should be removed for numerical efficiency. This is achieved by implicit treatment of the pressure gradient, of the mass fluxes in the mass conservation equations and of the equation of state.

The gradient of solid pressure in the solids momentum equations is also treated implicitly. It is basically the dependence of P_s on α that determines the stiffness of the problem, and hence the timestep restriction.

In view of the above restriction there is no need for other than explicit treatment of the convective terms; furthermore, in practice the timestep is chosen smaller than the Courant limit. Finally, slightly better resolution can be achieved with explicit TVD schemes compared to their implicit counterparts.

All terms associated with transfer processes between phases, i.e. mass momentum and heat transfer are treated implicitly, this decision being strongly dependent on the application. For example, the timescale associated with gas-particle drag interaction depends strongly on the particle diameter while the timescale of mass transfer depends on the temperature at which biomass pyrolysis occurs. However, implicit treatment of these term broadens the applicability of the code to other reactive multiphase systems, increasing its generality.

Finally, all diffusion processes are also treated implicitly. The timestep restrictions in the various equations are linear functions of the diffusion coefficients and inverse quadratic functions of the cellsize. In turbulent flow where diffusion coefficients may be appreciable, this may lead to restrictions, especially when the grid is heavily refined.

3.2 A model problem

A full discussion of the algorithm would be very lengthy. As the crux of the numerics lies in the solution of the hydrodynamic subproblem, we have chosen to illustrate the solution procedure for the mass, momentum and energy equations in absence of chemical reactions. We also restrict ourselves to a single particle class and exclude turbulence. We immediately give the discrete forms of the differential equations as these form the basis of the discussion of the iterative algorithm in the next subsection.

The mass conservation equation for phase k reads

$$\frac{(\alpha\rho)_k^{n+1} - (\alpha\rho)_k^n}{\Delta t} + L_h(M_k^{n+1}) = 0 \tag{100}$$

Here, L_h denotes the numerical divergence operator and M_k^{n+1} is the massflux vector $(\alpha\rho\mathbf{V})_k^{n+1}$. Note that the mass transfer terms are zero because of the absence of chemical reactions. Both model energy equations read

$$(\alpha\rho C_p)_g^n \frac{(T^{n+1} - T^n)_g}{\Delta t} + Q_g^T = L_h(\kappa_g G_h T_g^{n+1}) + K_{gs}^T (T_s - T_g)^{n+1} \tag{101}$$

and

$$(\alpha\rho C_p)_s^n \frac{(T^{n+1} - T^n)_s}{\Delta t} + Q_s^T = L_h(\kappa_s G_h T_s^{n+1}) + K_{gs}^T (T_g - T_s)^{n+1} \tag{102}$$

where the Q^T terms contain the (explicit) convective parts. Both the diffusion and the interphase transfer processes are treated implicitly. Further note that the diffusion factors κ are scalar coefficients. Finally, the discretized model momentum equations are

$$(\alpha\rho)^n \frac{(\mathbf{V}^{n+1}-\mathbf{V}^n)_g}{\Delta t} + Q_g = -\alpha_g^n G_h(P_g^{n+1}) + L_h(\mathbf{\Sigma}_g^*) + K_{gs}(\mathbf{V}_s - \mathbf{V}_g)^{n+1} + (\alpha\rho)_g^n \mathbf{g} \tag{103}$$

for the gas phase and

$$(\alpha\rho)^n \frac{(\mathbf{V}^{n+1}-\mathbf{V}^n)_s}{\Delta t} + Q_s = -\alpha_s^n G_h(P_g^{n+1}) - G_h(P_s^{n+1}) + L_h(\mathbf{\Sigma}_s^*) + K_{gs}(\mathbf{V}_g - \mathbf{V}_s)^{n+1} + (\alpha\rho)_s^n \mathbf{g} \tag{104}$$

for the solid phase. The convective part has been written non conservative; the motivation for this will be clear during discussion of the solution algorithm. G_h denotes the numerical gradient operator (Note: $G_h = L_h^T$). Again Q_k contain the explicit convective contributions for phase k. The star notation on the stress tensors Σ_k mean that they are handled in a mixed manner, i.e. the normal part is handled implicit while the transposed part is handled explicitly. This effectively decouples the x and y-momentum equations. Finally we have the two implicitly treated equations of state:

$$P_g^{n+1} = \rho_g^{n+1} R T_g^{n+1} \tag{105}$$

$$P_s^{n+1} = P_s(\alpha_2^{n+1}) \tag{106}$$

This completes the description of our model problem, the next subsection deals with the algorithm to solve it in an efficient and stable manner.

3.3 Solution algorithm

The algorithm basically consists of two steps. The first in which the energy equations are solved and where predictor values for the velocities are generated, the second which solely contains the iterative part of the algorithm and enforces mass conservation for all phases.

3.3.1 Step 1: Temperature solution and velocity prediction

First, the energy equations as discretized in equations (101,102) are solved for the new-time phase temperatures, T_k^{n+1}. The linear system arising from the discretization has the following form

$$\begin{bmatrix} \mathbf{A}_g^T & -\mathbf{K}_{gs}^T \\ -\mathbf{K}_{gs}^T & \mathbf{A}_s^T \end{bmatrix} \begin{bmatrix} \mathbf{T}_g^{n+1} \\ \mathbf{T}_s^{n+1} \end{bmatrix} = \begin{bmatrix} \mathbf{f}_g^T \\ \mathbf{f}_s^T \end{bmatrix} \tag{107}$$

Here, the submatrices $\mathbf{A}_k^T$ contain contributions from the time-derivative, phasic coupling and diffusion fluxes and have a standard 5-point structure. The submatrices $\mathbf{K}_{gs}^T$ are diagonal. This matrix is not a standard 5 (or 7 in 3D)-point matrix of size N. To avoid this complication, the so-called partial elimination algorithm (Oliviera and Issa, 1994) is usually employed where the dependency between the phases is algebraically eliminated leading to 2 systems having standard structure. However, this procedure is only formally correct on a point by point basis. It can not be done in full on the system as given above. We therefore do not resort to these approximations and solve the complete system (107). The detailed procedure is outlined below.

Second, the phasic coupled momentum equations in x and y-direction are solved using the old-time pressures to obtain predictor values of the U and V-velocities, U_k^*, and V_k^*, i.e. for the U-component write

$$(\alpha\rho)^n \frac{(U^*-U^n)_g}{\Delta t} + Q_g = -\alpha_g^n L^T(P_g^n) + L(\Sigma_g^*) + K_{gs}(U_s - U_g)^* + (\alpha\rho)_g^n \mathbf{g} \tag{108}$$

and

$$(\alpha\rho)^n \frac{(U^*-U^n)_s}{\Delta t} + Q_s = -\alpha_s^n L^T(P_g^n) - L^T(P_s^n) + L(\Sigma_s^*) + K_{gs}(U_g - U_s)^* + (\alpha\rho)_s^n \mathbf{g} \tag{109}$$

The purpose of the nonconservative form should now be clear. A conservative method would need the new time densities and volume fractions, both of which are unavailable at this time. The linear system again has the following form:

$$\begin{bmatrix} \mathbf{A}_g^U & -\mathbf{K}_{gs}^U \\ -\mathbf{K}_{gs}^U & \mathbf{A}_s^U \end{bmatrix} \begin{bmatrix} U_g^* \\ U_s^* \end{bmatrix} = \begin{bmatrix} \mathbf{f}_g^U \\ \mathbf{f}_s^U \end{bmatrix} \tag{110}$$

As illustrated above, the structure of the linear systems arising from the coupled energy equations and from the phasic coupled momentum equations is identical. Their numerical properties are also comparable, e.g. both are diagonally dominant due to the timestepping. This makes the linear systems suitable to iterative solution. Krylov methods have gained popularity for the solution of large sparse systems over the more classical iterative schemes (e.g. Golub and Van Loan, 1989). Because of its stability properties, we use GMRES (Saad and Schultz 1986) combined with suitably chosen preconditioners for the solution of these systems (Note that with GMRES we do not exploit the symmetry of the linear systems).

To enhance convergence, GMRES is applied to the preconditioned system

$$\mathbf{M}^{-1}\mathbf{A}\mathbf{x} = \mathbf{M}^{-1}\mathbf{b} \tag{111}$$

where $\mathbf{A}\mathbf{x} = \mathbf{b}$ denotes the original system and $\mathbf{M}$ is the preconditioner. $\mathbf{M}$ should approximate $\mathbf{A}$ at low cost and should be easily invertable (in GMRES several systems of the form $\mathbf{M}\mathbf{z} = \mathbf{y}$ need to be solved). In the present work $\mathbf{M}$ is approximated by the following matrix

$$\mathbf{M} = \begin{bmatrix} \mathbf{A}_g^* & -\mathbf{K}_{gs} \\ -\mathbf{K}_{gs} & \mathbf{A}_s^* \end{bmatrix} \tag{112}$$

where the $\mathbf{A}_k$ blocks have been approximated by their diagonals, i.e. $\mathbf{A}_k^* = \mathrm{diag}(\mathbf{A}_k)$. Hence, the preconditioner is obtained by neglecting the point to point coupling in the equations. The phasic coupling is however kept. As the phasic coupling is the dominant mechanism in the equations $\mathbf{M}$ tends to be a good approximation to $\mathbf{A}$. As already indicated, the preconditioning leads to systems of the form $\mathbf{M}\mathbf{z} = \mathbf{y}$. These systems are explicitly inverted on a point by point basis.

3.3.2 Step 2: mass conservation iteration

In step 2 of the overall algorithm, mass conservation will be enforced. Recall the discrete mass conservation equations

$$\frac{(\alpha\rho)_k^{n+1} - (\alpha\rho)_k^n}{\Delta t} + L_h(\alpha_k^{n+1}, \rho_k^{n+1}, V_k^{n+1}) = 0 \tag{113}$$

These relations constitute two field equations for the volume fractions (two fields), the velocities (two fields) and the gas density (one field). Note that obeys the summation rule: $\sum_k \alpha_k^{n+1} = 1$ and the gas density ρ_g^{n+1} is related to the gas pressure P_g^{n+1} and the new time temperature T_k^{n+1} by the equation of state (105). Furthermore, the velocity corrections can be related to corrections of gas pressure and solids pressure (or volume fraction via (106)). Therefore, the above mass conservation equations may be viewed as equations for the corrections to gas pressure, P_g' and volume fraction (e.g. α_s').

Normally, a link is made between velocity corrections and (gas-) pressure corrections. Here this link needs to be extended to include corrections to the solids pressure as well. It is well-known that these relations (to be derived from the discrete momentum equations) should include the effects of interphase momentum transfer. The link is established as follows.

Subtracting the predictor equation (108,109) from the 'desired' discretization (103,104) gives for the x-component of velocity (U) gives two coupled equations for the velocity corrections

$$(\alpha\rho)_g^n \frac{\Delta U_g}{\Delta t} = \underbrace{-\alpha_g^n G(\Delta P_g)}_{D_g} + K_{gs}(\Delta U_s - \Delta U_g) \tag{114}$$

and

$$(\alpha\rho)_s^n \frac{\Delta U_s}{\Delta t} = \underbrace{-\alpha_s^n G(\Delta P_g) - G(\Delta P_s)}_{D_s} + K_{gs}(\Delta U_g - \Delta U_s) \tag{115}$$

The D_k terms are the 'driving forces' behind the corrections. Note that the viscous parts have been neglected in the subtraction (See Van Kan (1986) for a formal justification). Rearranging the equations gives

$$\begin{bmatrix} H_g + K_{gs} & -K_{gs} \\ -K_{gs} & H_s + K_{gs} \end{bmatrix} \begin{bmatrix} \Delta U_g \\ \Delta U_s \end{bmatrix} = \begin{bmatrix} D_g \\ D_s \end{bmatrix} \tag{116}$$

where we have used the shorthand H_k for the time related coefficient $(\alpha\rho)_k^n \Delta t$. This system can be solved analytically to reveal the relation between the velocity corrections and both pressure corrections. This may be considered a generalization of relations usually found in literature in the absence of solids pressure. (see e.g. Oliviera and Issa, 1994).

As the mass conservation equations are nonlinear, some form of iteration needs to be implemented. Several possibilities may be identified:

1. Distributive iteration.

   This is a general term for iterative schemes that in some way rely on subsequent solution of equations. To be more specific, one may successively solve the solids volume fraction from the solids mass equation and solve gas pressure from the imbalance in the gas mass equation. This is only one example from many schemes found in literature. Note that decoupled iterations are usually imbedded in the overall iterative scheme taking place over all of the equations. Hence, these methods are strongly related to the SIMPLE class of algorithms.

2. Newton's method and approximate Newton.

   Writing all variables as their present approximation and a correction and neglecting products of corrections leads to a linear system for the simultaneous volume fraction and gas pressure corrections. This linear system is sparse. When implemented concisely, this scheme converges

quadratically and only 2 or 3 'linearize and solve' steps are necessary. There is however one main drawback to this scheme: when the TVD scheme is used for the convection approximation the exact linearizations are very awkward to derive and increase the stencil compared to the upwind scheme. A simpler approach was followed by Lathouwers and Van den Akker (1996) where inexact linearizations were used. The drawback is that quadratic convergence is lost.

3. Nonlinear multigrid iteration.

   The nonlinear multigrid algorithm is the most general iterative approach to the solution of nonlinear problems. It is not as widely used as the linear variant, mostly due to the complexity of implementing such a scheme. There are however examples in fluid mechanics where enormous speedups have been reported compared to single grid methods. A very important property of the iterative method is that the reduction factors are independent of the gridsize, i.e. the amount of work increases linearly with the number of unknowns.

The third option has been implemented in the present code. The reader is referred to the standard literature on multigrid methods for the standard nonlinear algorithm (Wesseling, 1992). The most important ingredient of a multigrid algorithm is the smoother used to smooth the residual. Here, one smoothing step consists of a linearization of the equations in terms of the fraction and pressure correction. After that, an alternating 'zebra' Gauss Seidel solver is used to smooth the error (Wesseling, 1992). Note that solving for the fraction and pressure corrections on a line leads to a band matrix (bandwidth: 7 for 1 particle class, 11 for 2 particle classes). All other components of the multigrid algorithm as used here are fairly standard (e.g. injection as restriction operator and second order prolongation).

4 A validation study

In this section we present a qualitative validation study of a bubbling fluidized bed. The main objective of this study is to see whether the main characteristics of a bubbling bed can be predicted with the kinetic theory model and if the numerical approach works stable and efficient for a flow problem of this type. Therefore, a bed is studied that is stripped from most of the complications that have been discussed in the modeling section, i.e. a single particle class system is studied without chemical reactions and turbulence.

4.1 Geometry, physical model, and boundary conditions

The geometry consists of a two-dimensional dense fluidized bed of $0.8\,m$ wide and $1.25\,m$ high. Initially, the bed is filled with typical sand particles with diameter $d_p = 500\,\mu m$ and density $\rho_p = 2500\,kg/m^3$ to a height of about $0.5\,m$ 'Filled' in this respect means that the particle volume fraction is prescribed at 0.6 which is close to the maximum packing of solids corresponding to a volume fraction of 0.64 The coefficient of restitution is empirically set to 0.9. The fluidized bed is uniformly aerated at the bottom with a superficial gas velocity of $1\,m/s$. Note that this is well above the minimum fluidization velocity, V_{mf}, which is approximately $0.25\,m/s$. The bed is therefore expected to be in the bubbly flow regime.

In the case study under consideration, only a single particle class is present. Following the above model for the binary mixture, the particle distribution function has been chosen as Gaussian. Furthermore, turbulence in the carrier-phase is neglected in this simplified simulation. The model

then becomes equal to that presented by Ding and Gidaspow (1990). Here we apply this model to the bubbling fluidized bed under the conditions outlined above.

The equations are discretized on a uniform 30 times 76 in the horizontal and vertical directions respectively. This is a typical resolution for bubbling fluidized beds discussed in the literature. The appropriate boundary conditions specified are: at the inlet, the gas fraction is set to unity and its velocity equal to the superficial velocity; at the top of the bed, the gas pressure is fixed to be atmospheric; at the side walls, both gas-phase components are set to zero (no-slip condition), while the solids are allowed to slip freely along the wall (no shear stress). This is consistent with the assumption of a Gaussian velocity distribution for the particle velocity. A run of 10000 timesteps has been performed with the timestep fixed at $2.10^{-4}s$.

The new numerical algorithm performed well during the simulation and did not show any instabilities. Calculations of this type are inherently intensive due to the transient behavior and the required implicitness in the algorithm; the simulations described above required several hours of computing time on a Cray J90. Furthermore, it appears that the resolution used in the present simulation is insufficient to support all the details of the flow.

4.2 Results and discussion

The calculations are started with a slight nonuniformity in the solids volume fraction: more specifically, the solids volume fraction at the left hand side of the bed is set to 0.5 rather than 0.6. This inhomogeneity is induced to speed up the development of the flow toward the bubbly regime. Similar procedures to reduce start-up time are reported in literature (Peirano, 1998). Results at different stages of the simulation are depicted in Figures 1 to 4. In these figures, contours of the solids volume fraction and the velocity fields of both the gas and solid phases are shown. At start-up, the gas flow at the distributor pushes the solids upward and creates a layer of somewhat more compacted solids. At the same time, a gas layer is created at the bottom of the bed. Owing to the form of the drag interaction, the particle slip velocity in a dilute region is higher than in a compacted region. Therefore, the solids start to fall down towards the distributor through the formed gas layer. This in turn creates a more compacted region at the distributor which is subsequently convected upwards due to the increased drag with the gaseous phase. This process repeats itself and several layers can be can be identified in figure 2, with increasing number of layers in figure 3. These layers are mostly restricted to the right hand side of the bed as the left hand side is perturbed due to the initial conditions used for the solids volume fraction.

At 0.4 s of physical time (figure 1) the velocity fields of both phases are still spatially uniform. As time proceeds, the perturbations induced at the left hand side start to effect the remainder of the bed. In particular, at 0.8 seconds after start-up the first void region ('bubble') is formed in the lower left corner. This 'bubble' has not only a local effect but affects the entire bed. It can be seen from figure 2 (and subsequent figures) that the gaseous phase prefers to flow through the void regions rather than through the bed; obviously, the reduced drag in these regions plays an important role. The process of layer formation just described persists in the right hand side of the domain, and as a result, the bed expands appreciably as can be seen from figure 3 where the bed is at its maximum expansion. This also has consequences for the numerical domain that is to be used in the computations, as too short a domain will result in a loss of particles.

At approximately 1.5 seconds after start-up of the fluidized bed, the solid phase at the top of the bed is sufficiently diluted and an approximately statistically steady situation is reached. At this point, the disturbances have reached the right hand side of the bed and an unsteady motion is seen throughout the bed with both void and dense regions. In most parts of the bed the solids volume

fraction is above 40 % while in the void regions the solids fraction is generally below 5 %. Throughout the bed the velocity fields of the phases exhibit circulating motion. The circulating motion of the solid phase is responsible for sustaining the particle fluctuating motion. This fluctuating motion in turn gives rise to a 'particle pressure' which partially carries the weight of the solids in the bed and prevents local overcompacting. The circulatory motion confirms our intuition that $k-\varepsilon$ models for the gas phase are inappropriate (Wilcox, 1994).

This granular temperature varies significantly throughout the bed, from almost zero in the freeboard where velocity gradients are absent (see e.g. figure 3 and 4) to approximately 10^{-5} in the dense regions of the bed. The low granular temperature as predicted by the model in the dilute region is unrealistic and is due to the approximation of the distribution function as Gaussian; one would normally expect the highest granular temperature in those regions. Our further steps in this modeling effort will remove the Gaussian assumption.

Although no quantitative comparisons are made at this point, the qualitative behavior of the fluidized bed is well reproduced exhibiting transient flow even with steady state, uniform boundary conditions. Furthermore, both dense and void regions are predicted. It is therefore concluded that evan a simplified kinetic theory of dense gases applied to the flow of particles in a gas is capable of predicting the behavior of bubbling fluidized beds (at least qualitatively). This conclusion is expected to prevail for the binary mixture. Future work will focus on model improvement for quantitative predictions.

5 Conclusions and future work

A mathematical model has been presented which is capable of predicting the (thermo) fluid dynamics of biomass pyrolysis in a fluidized bed reactor. The model will be used for situations where the biomass particles are small enough to have the pyrolysis occuring in the kinetic regime, i.e. diffusion limitations are assumed negligible. The rate at which pyrolysis occurs is, however, determined by the rate at which heat can be supplied by the sand and the carrier gas.

The model comprises of a systematic derivation of the continuum equations of the gaseous and solids phases which is the most suitable for the present application. Separate averaging procedures have been outlined and applied to the gas and particulate phases leading to macroscopic equations requiring closure relations to obtain a solvable system.

For the gas phase, closure is provided along the lines of the extension of single particle class results to the presence of two different solids. Furthermore, exchange terms with the solid phases are incorporated expressing mass, heat and energy transfer. Gas phase turbulence is accounted for by the inclusion of a stress transport model which is modeled after single-phase flow closures but with some extension to account for the presence of the particles.

On the other hand, for the solids, closure is provided for by using the framework of kinetic theory of binary granular media, extended here to partly include the presence of an interstitial gas. In this framework the particles are modelled as slightly inelastic spheres. All closure relations are written in terms of the single particle distribution functions which are solutions to the respective Boltzmann equations. At the present time Gaussian approximations to these distributions have been made. The collisional transfer includes the heat transfer between sand and biomass particles.

As the model describing the process is both nonuniform and transient, calculations are computationally intensive. Furthermore, the equations are very stiff due to the various timescales in the problem. Therefore, a both efficient and robust numerical algorithm is needed to obtain reasonable computational times and stable integration. Such an algorithm has been presented, and has been shown to work well in the test case considered.

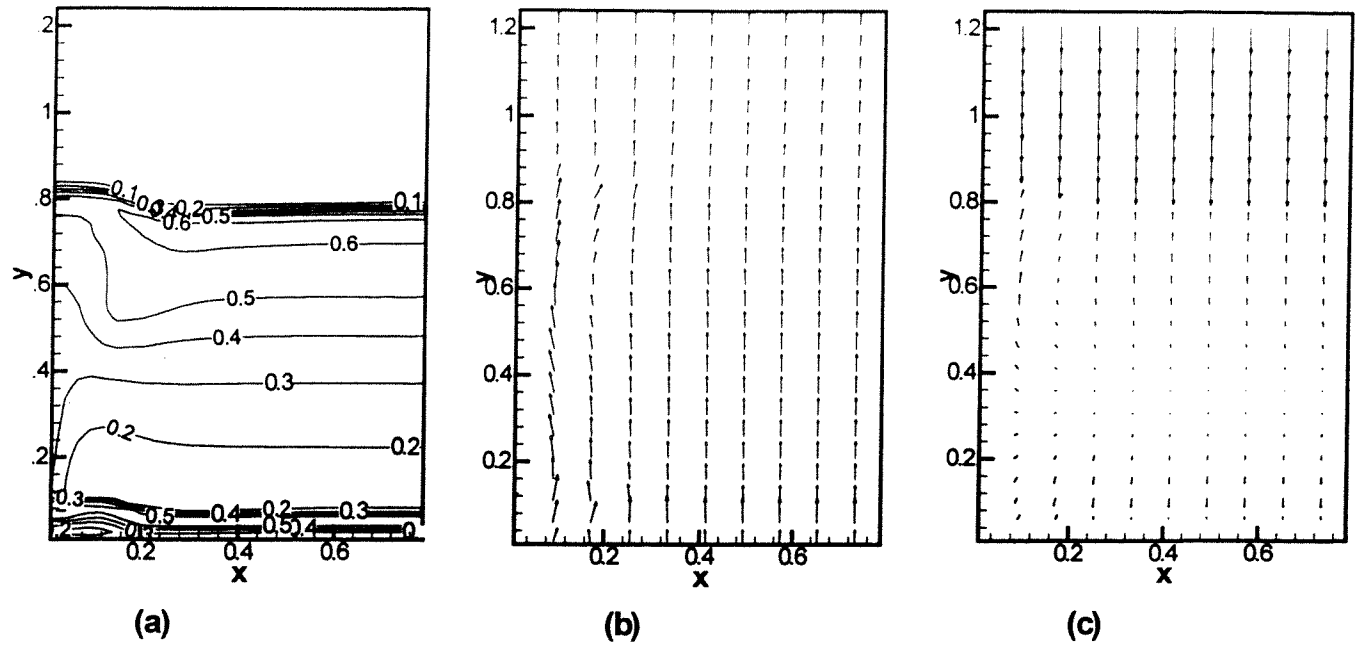

Figure 1: Contours of the solids volume fraction (a), velocity vectors of the gas phase (b) and of the solid phase (c) at 0.4 s. after startup.

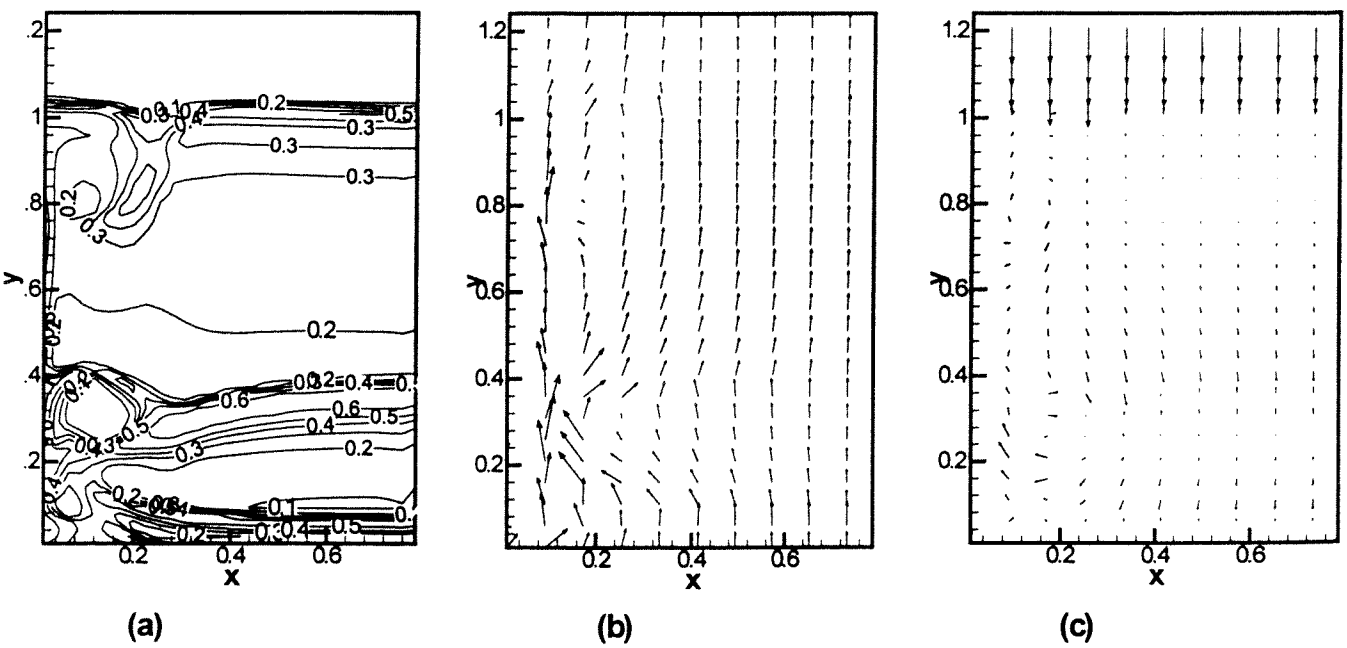

Figure 2: Contours of the solids volume fraction (a), velocity vectors of the gas phase (b) and of the solid phase (c) at 0.8 s. after startup.

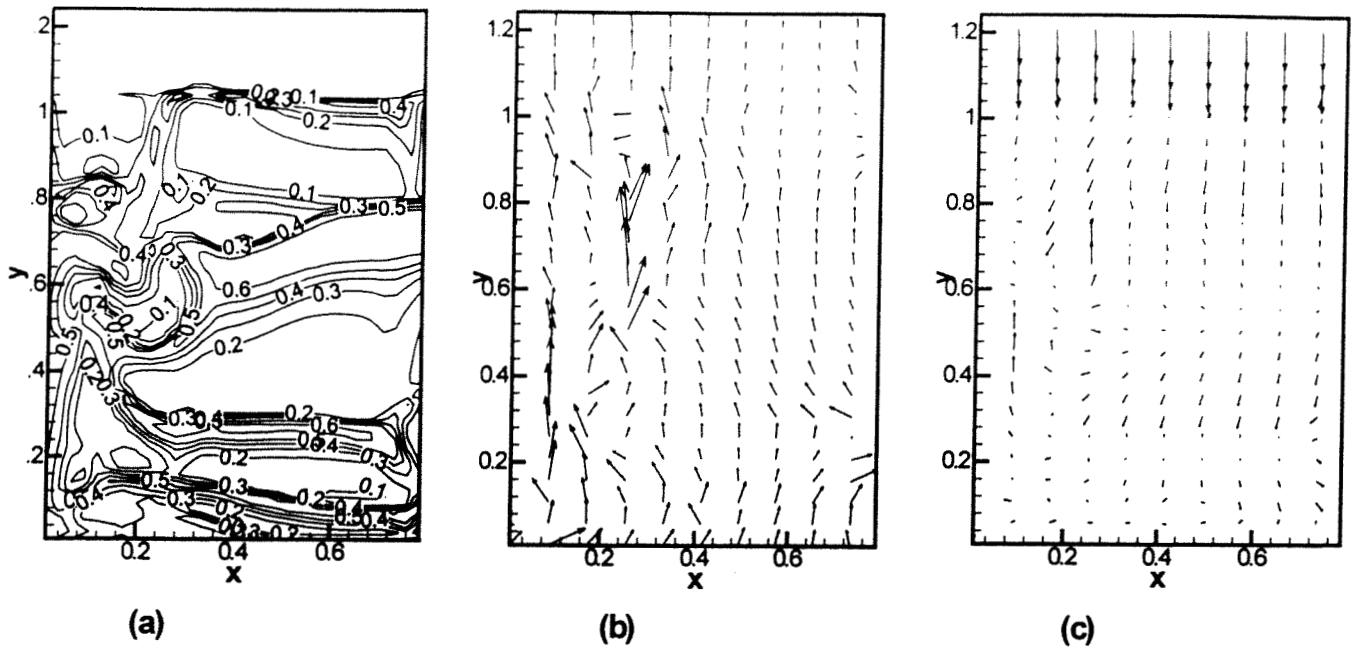

Figure 3: Contours of the solids volume fraction (a), velocity vectors of the gas phase (b) and of the solids phase (c) at 1.2 s. after startup.

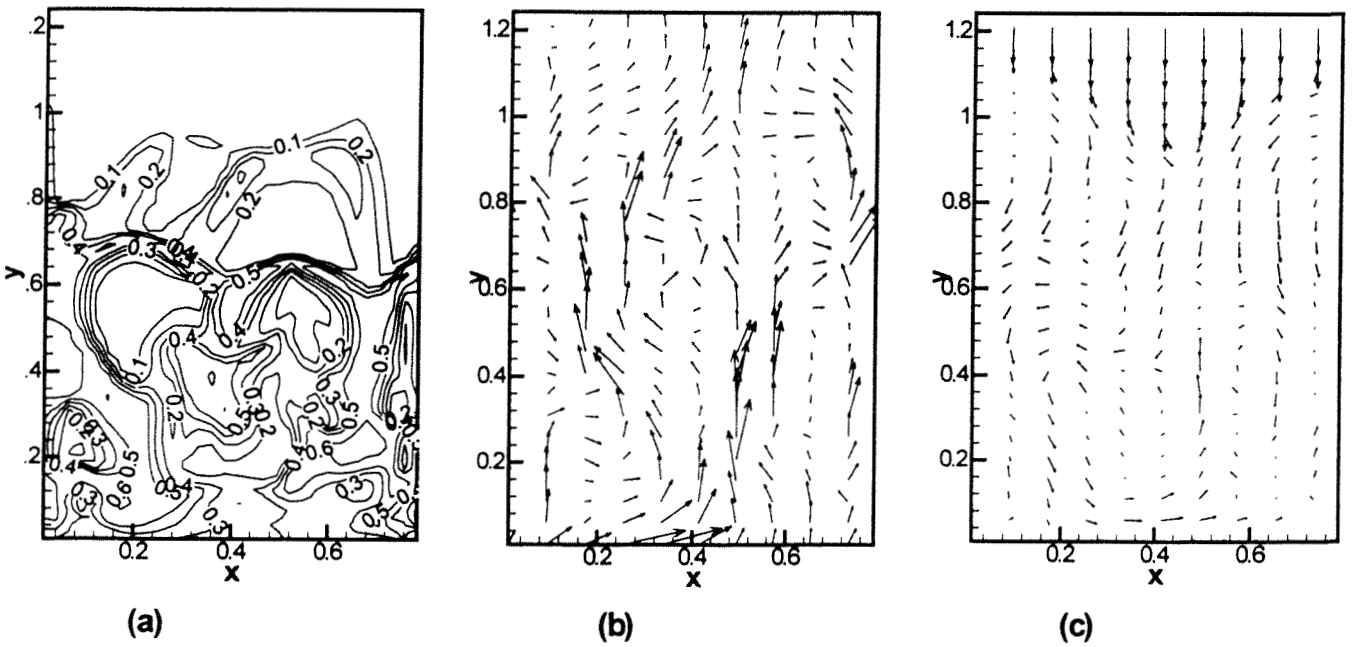

Figure 4: Contours of the solids volume fraction (a), velocity vectors of the gas phase (b) and of the solid phase (c) at 1.8 s. after startup.

This test case consisted of a two-dimensional bubbling fluidized bed, uniformly aerated at the bottom section. All solid particles in the bed belonged to the same particle class. Although this test case constitutes a simplification of the complete model, it does produce results in qualitative agreement with experiments predicting both transient flow arising from physical instabilities, observed flow patterns, and 'bubble' (regions having few particles) formation, even when uniformly aerated.

Future developments include the extension of the above model to non-Gaussian distribution functions for the particle phases which will lead to a more accurate description in the dilute region of the fluidized bed reactor and will allow for a more detailed analysis of the effect of the carrier gas on the particles. This extension will be made along the lines of Grad's theory (see Peirano, 1998), extended to a binary granular mixture.

The model will first be validated against suitable pyrolysis experiments (Scott et al., 1988; Stiles and Kandiyoti, 1989) to verify its predictive capabilities. As it is formulated, the model is well suited for the optimization of reactor geometries and operating parameters, such as operating temperature, injection procedures, etc. and the present model will be used to optimize the NREL fluidized bed pyrolysis reactor.

6 Acknowledgments

This research was conducted at the Jet Propulsion Laboratory (JPL) and sponsored by the U.S. Department of Energy (DOE), with Mr. Neil Rossmeisel (DOE Headquarters) and Mr. D. Hooker (DOE Golden Center) serving as contract monitors, under an agreement with the National Aeronautics and Space Administration. Computational resources were provided by the supercomputing facility at JPL. The authors wish to thank Dr. R. S. Miller for useful discussions on biomass pyrolysis and Dr. K. G. Harstad for helpful discussions on kinetic theory.

References

[1] Balzer, G. and Simonin, O. 1993. *Extension of Eulerian Gas-Solid Flow Modelling to Dense Fluidized Bed.* EDF Technical Report HE-44/93.13 B.

[2] Bolio, E.J. and Sinclair, J.L. 1995. *Gas Turbulence Modulation in the Pneumatic Conveying of Massive Particles in Vertical Tubes.* Int. J. Multiphase Flow 21(6):985-1001.

[3] Bulthuis, H.F. 1997. *Dynamics of Bubbly Flows.*, PhD. thesis, Twente University of Technology, The Netherlands.

[4] Campbell, C.S. 1991. *Rapid Granular Flows.* Ann. Rev. Fluid Mech.

[5] Chapman, S. and Cowling, T.G. 1970. *The Mathematical Theory of Nonuniform Gases.* Cambridge University Press.

[6] Daly, B.J. and Harlow, F.H. 1970. *Transport Equations in Turbulence.* Physics of Fluids 13:2634-2649.

[7] Ding, J. and Gidaspow, D. 1990. *A Bubbling Fluidization Model using Kinetic Theory of Granular Flow.* AIChE Journal 36(4):523-538.

[8] Drew, D.A. 1983. *Mathematical Modeling of Two-Phase Flow.* Ann. Rev. Fluid Mech. 15:261-291.

[9] Farell, M., Lun, C.K.K and Savage, S.B. 1986. *A Simple Kinetic Theory for Granular Flow of Binary Mixtures of Smooth, Inelastic, Spherical Particles.* Acta Mechanica 63:45-60.

[10] Gibson, M.M. and Launder, B.E. 1978. *Ground Effects on Pressure Fluctuations in the Atnospheric Boundary Layer.* J. Fluid Mech. 86:491

[11] Gidaspow, D. 1986. *Hydrodynamics of Fluidization and Heat Transfer: Supercomputer Modeling.* Appl. Mech. Rev. 39(1):1-22.

[12] Golub, G.H. and Van Loan, C.F. 1989. *Matrix Computations.* Johns Hopkins University Press.

[13] Grad, H. 1949. *On the Kinetic Theory of Rarefied Gases.* Comm. Pure and Appl. Math. 2:331-407.

[14] Hirsch, C. 1990. Numerical Computation of Internal and External Flows. Volume 2. Wiley.

[15] Jenkins, J.T. and Savage, S.B. 1983. *A Theory for the Rapid Flow of Identical, Smooth, Nearly Elastic, Spherical Particles.* J. Fluid Mech. 130:187-202.

[16] Jenkins, J.T. and Richman, M.W. 1985. *Grad's 13-Moment System for a Dense Gas of Inelastic Spheres.* Arch. Rat'l Mech. Anal. 87:355-377.

[17] Jenkins, J.T. and Mancini, F. 1987. *Balance Laws and Constitutive Relations for Plane Flows of a Dense, Binary Mixture of Smooth, Nearly Elastic, Circular Disks.* Journal of Applied Mechanics. 54:27-34.

[18] Jenkins, J.T. and Mancini, F. 1987. *Kinetic Theory for Binary Mixtures of Smooth, Nearly Elastic Spheres.* Phys. Fluids A 1(12):2050-2057.

[19] Lathouwers, D. and Van den Akker, H.E.A. 1996. *A Numerical Method for the Solution of Two-Fluid Model Equations.* Numerical Methods in Multiphase Flows 1996. (Ed. Crowe, C.T.), ASME.

[20] Louge, M., Yusof, J.M. and Jenkins, J.T. 1993. *Heat Transfer in the Pneumatic Transport of Massive Particles.* Int. J. Heat Mass Transfer. 36(2):265-275.

[21] Van Kan, J. 1986. *A Second-Order Accurate Pressure Correction Scheme for Viscous Incompressible Flow.* SIAM J. Sci. and Stat. Comput. 7(3):870-891.

[22] Lun, C.K.K., Savage, S.B., Jeffrey, D.J. and Chepurniy, N. 1984. *Kinetic Theories for Granular Flow: Inelastic Particles in Couette Flow and Slightly Inelastic particles in a General Flowfield.* J. Fluid Mech. 140:223-256.

[23] Mathiesen, V., Solberg, T., Manger, E. and Hjertager, B.H. 1996. Modelling and Predictions of Multiphase Flow in a Pilotscale Circulating Fluidized Bed. 5th Int. Conf. on CFB, Int. Chem. Metallurgy, Bejing, May 28-June 1, MSD5 1-6.

[24] Miller, R.S. and Bellan, J. 1997. *A Generalized Biomass Pyrolysis Model Based on Superimposed Cellulose, Hemicellulose and Lignin Kinetics.* Combust. Sci. and Tech., 126:97-137.

[25] Miller, R.S. and Bellan, J. 1998. *Numerical Simulation of Vortex Pyrolysis Reactors for Condensable Tar Production from Biomass. Energy & Fuels.*, 12:25-40.

[26] Miller, R.S., Harstad, K. and Bellan, J. 1998. *Evaluation of Equilibrium and Non-Equilibrium Evaporation Models for Many-Droplet Gas-Liquid Flow Simulations.* Int J. Multiphase Flow. 24:1025-1055.

[27] Oliviera, P.L. and Issa, R.I. 1994. *On the Numerical Treatment of Interphase Forces in Two-Phase Flows.* Numerical Methods in Multiphase Flows 1994. (Ed. Crowe, C.T.), ASME.

[28] Peirano, E. 1998. *Modelling and Simulation of Turbulent Gas-Solid Flows applied to Fluidization.* PhD. thesis, Chalmers University of Technology.

[29] Rivard, W.C. and Torrey, M.D. 1977. K-FIX: *A Computer program for Transient, Two-dimensional, Two-fluid Flow.* Internal Report Los Alamos, LA-NUREG-6623.

[30] Saad, Y. and Schultz, M.H. 1986. GMRES: *A Generalized Minimum Residual Algorithm for Solving Non-Symmetric Linear Systems.* SIAM J. Sci. and Stat. Comput. 7:856-869.

[31] Scott, D.S. et al. 1988. *The Role of Temperature in the Fast Pyrolysis of Cellulose and Wood.* I&EC Research 27:8-15.

[32] Stiles, N.H. and Kandiyoti, R. 1989. *Secondary Reactions of Flash Pyrolysis Tars Measured in a Fluidized bed Pyrolysis Reactor with some Novel Design Features.* Fuel 68:275-282.

[33] Syamlal, M. 1997. *Higher Order Discretization Methods for the Numerical Simulation of Fluidized Beds.* Fluidization and Fluid-Particle Systems Topical Conference, AIChE Annual Meeting, Los Angeles, 1997.

[34] Syamlal, M. 1998. *MFIX Documentation Numerical Technique.*

[35] Tamamidis, P. and Assanis, D. 1993. *Evaluation of Various High-Order Accuracy Schemes with and without Flux Limiters.* Int. J. Num. Meth. Fluids 16:931-948.

[36] Tham, M.K. and Gubbins, K.E. 1971. *Kinetic Theory of Multicomponent Dense Fluid Mixtures of Rigid Spheres.* J. Chem Phys. 55(1):268-279.

[37] Wesseling, P. 1992. *Introduction to Multigrid Methods.* Wiley.

[38] Wilcox, D.C. 1994. *Turbulence Modeling for CFD.* DCW Industries, Inc.

[39] Zha, G. and Knight, D. 1996. AIAA J. 34(7):1313-1320.

[40] Zhang, D.Z. and Prosperetti, A. 1997. *Momentum and Energy Equations for Disperse Two-Phase Flows and Their Closure for Dilute Suspensions.* Int. J. Multiphase Flow 23(3):425-453.